

# 1 **Modelling evaporation with local, regional and global BROOK90** 2 **frameworks: importance of parameterization and forcing.**

3 Ivan Vorobevskii, Thi Thanh Luong, Rico Kronenberg, Thomas Grünwald, Christian Bernhofer  
4 Faculty of Environmental Sciences, Department of Hydrosociences, Institute of Hydrology and Meteorology, Chair of  
5 Meteorology, Technische Universität Dresden, Tharandt, 01737, Germany  
6 *Correspondence to:* Ivan Vorobevskii (ivan.vorobevskii@tu-dresden.de)

## 8 **Abstract.**

9 ~~Evaporation plays an important role in the water balance on a different spatial scales. Observation and estimation of evaporation~~  
10 ~~is a challenging task. Evaporation occurs on each surface and is driven by different energy sources. However, its direct and~~  
11 ~~indirect measurements are globally scarce and accurate estimations are a challenging task. Thus For the correct process~~  
12 approximation in modelling of the terrestrial ~~water balance~~ evaporation plays a crucial part is still difficult. Here, we use a  
13 physically-based 1D lumped soil-plant-atmosphere model (BROOK90) is applied to study the role of parameter selection and  
14 meteorological input forcing for the simulation modelled of evaporation on at the point scale. Then, with By the integration of  
15 the model into global, regional and local frameworks, we made cross-combinations were elaborated out of their  
16 parameterization and forcing schemes to ~~analyse the associated model uncertainty~~ show analyse and analyse show their roles in  
17 the estimations of the evaporation.

18 Five sites with different land uses (grassland, cropland, deciduous broadleaf forest, two evergreen needleleaf forests) located  
19 in Saxony, Germany were selected for the study. ~~All combinations of the model setups were validated using FLUXNET data~~  
20 ~~and various goodness of fit criteria. The output from a calibrated model with in situ meteorological measurements served as a~~  
21 ~~benchmark. We focused on the analysis of the model performance with regard to different time scales (daily, monthly, and~~  
22 ~~annual). Additionally, components of evaporation are addressed, including their representation in BROOK90. Finally, all~~  
23 ~~results are discussed in the context of different sources of uncertainty: model process representation, input meteorological data~~  
24 ~~and evaporation measurements themselves. All tested combinations showed a good agreement with FLUXNET measurements~~  
25 (KGE values 0.35-0.80 for a daily scale). For most of the sites, the best results was found for the calibrated model with in situ  
26 meteorological input data, while the worst was observed for the Global BROOK90 with ERA5 global setup forcing. The  
27 setups' performance in the vegetation period was much higher than for the winter period. Among the tested setups, the model  
28 parameterisation gave showed lead to a higher spread in the model performance than it was observed due to the meteorological  
29 forcings for fields and evergreen forests sites, while opposite was noticed in deciduous forest. The Aanalysis of the of  
30 evaporation components revealed that transpiration dominates (up to 65-75 %) in the vegetation period, while interception (in  
31 forests) and soil/snow evaporation (in fields) prevails in the winter months. Finally furthermore, it was found that different

32 ~~parameter sets impact the model performance and redistribution of evaporation components throughout the whole year, while~~  
33 ~~the influence of meteorological forcing was evident only in summer months. Finally, the results suggest that ERA5~~  
34 ~~data might serve as reasonable meteorological forcing for evaporation simulations even at a local, respectively point scale.~~

## 35 1 Introduction

36 Evaporation as a water balance component plays an important role in the hydrological process at multiple spatial scales: from  
37 a single leaf to an entire catchment. As a result of mass and energy exchange between the soil-plant and atmosphere system,  
38 the global annual terrestrial evaporation amount yields approximately  $\frac{2}{3}$  of the total precipitation (McDonald, 1961), ~~showing~~  
39 ~~however large range even on a macroscale~~ (Haddeland et al., 2011; Harding et al., 2011; Miralles et al., 2016). However, with  
40 the need of higher spatial and temporal resolution, ~~the high variability of evaporation should be taken into account and properly~~  
41 ~~addressed evaporation exposes larger variability~~ (Anderson et al., 2007; Baldocchi et al., 2001; Jung et al., 2011; Pan et al.,  
42 2020; Zhang et al., 2010). Thus, accurate estimates of evaporation on different scales as well as ~~deepening knowledge advanced~~  
43 ~~understanding~~ of the process itself, are beneficial for planning, developing and monitoring of hydrologic, agriculture and  
44 ecological systems, e.g., irrigation scheduling, water distribution systems, crop modelling, quantification of energy and  
45 moisture exchange between the land surface and the atmosphere (Fisher et al., 2017; McNally et al., 2019; Schulz et al., 2021).  
46 Apart from the total evaporation itself, it is sometimes necessary to assess and quantify its components (Chang et al., 2018;  
47 Lawrence et al., 2007; Leuning et al., 2008; Schulz et al., 2021), namely components, like transpiration, evaporation from the  
48 ground or snow surface, and evaporation of intercepted rain and snow from the canopy. ~~However the partition of the~~  
49 ~~evaporation is a subject of a large variability and depends not only on the location, but on scale as well~~ (Wei et al., 2017; Zhang  
50 ~~et al., 2017~~).

51 Various direct (i.e. porometer, eddy-covariance ~~and~~ lysimeter) and indirect (~~Bowen ratio, gradient, experimental water balance~~  
52 ~~watershed catchment water balance, energy balance, theoretical models based on meteorological data~~) methods have been  
53 developed and used to measure evaporation at different spatio-temporal scales. Each method has its strengths and weaknesses,  
54 but what they have in common is that the results ~~have limited representativeness. Namely, they~~ are valid only within a ~~certain~~  
55 ~~space of scale and time. This (so-called "footprint"), which~~ is usually quite small, thus only a local scale could be represented  
56 by it (Baldocchi, 1997; Wilson et al., 2001). Recently, these methods were extended to include remote sensing techniques for  
57 the regional and global scale (Anderson et al., 2008; Leuning et al., 2008; Miralles et al., 2011, 2016), but the quality of the  
58 output products possess still a potential for improvement (Pan et al., 2020; Zeng et al., 2012). Among the ~~operational~~  
59 ~~measurements datasets of the in-situ evaporation measurements~~, the FLUXNET ~~network~~ (<http://www.fluxnet.ornl.gov>) ~~project~~  
60 ~~has the largest network with provides eddy-covariance data from~~ about 500 stations worldwide ~~within FLUXNET2015 dataset~~  
61 (Pastorello et al., 2020) ~~The project allocates standardized eddy-covariance techniques since 1990s, and is and~~ still ~~acting acts~~  
62 as ~~the~~ main driver in advancing evaporation research (Baldocchi et al., 2001; Jung et al., 2011; Mauder et al., 2018).

Отформатировано: немецкий (Германия)

Отформатировано: английский (Соединенное Королевство)

Отформатировано: английский (Соединенное Королевство)

63 Evaporation measurements are still scarcely available due to high costs and the problem of large-scale representability (in  
64 comparison to e.g. discharge measurements).

65 Hence, mathematical modelling in favour of its feasibility is a practical substitute. Besides empirical formulas (Cerro et al.,  
66 2021; Feng et al., 2016; Zeng et al., 2012), evaporation is often estimated by physically-based models (Beven et al., 2021;  
67 Boulet et al., 2015; Liu et al., 2012; Mallick et al., 2018), in which Penman-Monteith (and Shuttleworth and Wallace extension)  
68 formula is one of the most frequently used. This approach reduces potential evaporation to an actual one accounting for the  
69 available water in the soil-plant system. Thus, it is incorporated into many land surface models and frameworks regardless of  
70 scale: local, regional or even global (Leuning et al., 2008; Mallick et al., 2018; Zink et al., 2017). Despite many efforts to  
71 improve evaporation models on different scales, large uncertainties still remain (Allen et al., 1998, p.56; Miralles et al., 2016,  
72 p.2; Mueller et al., 2011) (Allen et al., 1998; Miralles et al., 2011; Mueller et al., 2011). In general, the sources of evaporation  
73 modelling (or more in general – hydrological modelling) uncertainties can be classified as following: model structure and  
74 process representation, choice of an appropriate parameter set, meteorological input data, spatio-temporal miss-scaling and  
75 uncertainties of evaporation measurements for the model validation themselves (Mallick et al., 2018; Mauder et al., 2018;  
76 Mueller et al., 2011; Zhang et al., 2010). Studying these sources of uncertainties from different approaches and frameworks  
77 gained more attention in recent years, however most of these studies are limited by the focus on one single spatio-temporal  
78 scale (Chang et al., 2018; Jung et al., 2011; Liu et al., 2012). Only a few researchers focused on clarifying investigations of  
79 the uncertainties in multiple frameworks with multiple input datasets and simultaneously accounting for point, regional and  
80 global scales (Pan et al., 2020; Su et al., 2005; Winter and Eltahir, 2010).

81 Here we aim to extend the knowledge of uncertainty in evaporation modelling by analysing the output of on evaporation  
82 estimations based on the soil-plant-atmosphere physically-based lumped BROOK90 model, which we integrated into three  
83 different frameworks. These frameworks use different “state-of-the-art” sources of data for the model parameterisation and  
84 forcing which represent various spatial scales. Namely these scales are global, regional and local. By mixing these different  
85 datasets and validating the simulated evaporation with eddy-covariance measurements, we show want to show dependencies  
86 of the spatial scale of BROOK90 model parameterization and forcing data on the accuracy of evaporation simulation estimates.  
87 Our main hypothesis is that the goodness of fit of the setups smoothly increases from global to local scale (for both with respect  
88 to the- parameterization and as well as to the forcing). However, it was unclear how the scale combinations will perform, i.e.  
89 local meteorological data with global parameterization and vice versa. Therefore, this study presents the first qualitative  
90 analysis of the model input scale uncertainty uncertainty in general exemplarily, based on the best- globally available and locally  
91 available data sets. not going into deep quantitative quantitative analysis of single uncertainties using i.e. e. statistical  
92 bootstrapping or Monte-Carlo simulations. Therefore, this studyIt also possesses a practical outcome. Namely in a presence of  
93 limited resources and data, first conclusions can be drawn about the reliability of evaporation estimates for a point (hydrological  
94 response unit) scale can be drawn by from can the global or regional BROOK90 frameworks. Moreover, the study points to a

Отформатировано: английский (Соединенное Королевство)

Отформатировано: немецкий (Германия)

Отформатировано: не выделение цветом

Отформатировано: не выделение цветом

Отформатировано: не выделение цветом

Отформатировано: не выделение цветом

Отформатировано: не выделение цветом

Отформатировано: не выделение цветом

Отформатировано: не выделение цветом

Отформатировано: не выделение цветом

Отформатировано: не выделение цветом

95 ~~direction and where the BROOK90 user should put more attention – accurate parameterization or meteorological input. analyse~~  
96 ~~which aspect of the framework possesses more uncertainty. In this study, we focus on its two potential sources – the parameter~~  
97 ~~set or the meteorological input.~~ Thus, the outcome of this study aims to provides a better understanding of the BROOK90  
98 model as well as the ~~results should show~~s the directions to improve effectively evaporation simulations.

Отформатировано: не выделение цветом

Отформатировано: не выделение цветом

Отформатировано: не выделение цветом

## 100 ~~Data~~Material and methods

### 101 2.1 Study sites and Eddy-covariance measurements

102 The evaluation of simulated evaporation was carried for five sites with various land covers and long-term eddy-covariance  
103 measurements (Fig. 1, Table 1). All selected towers are located in Saxony, Germany. The study area is characterized by  
104 temperate suboceanic/subcontinental climate (Cfb, Kottek et al., 2006). The average mean daily temperature varies between  
105 ~~±15~~ °C and ~~+20±5~~ °C in summer months and between -5 °C and +5 °C in winter months. The average annual precipitation  
106 varies between 750 mm and 960 mm. The measurements of atmospheric fluxes with standardized methods are operated by  
107 Technische Universität Dresden within ICOS and FLUXNET projects. In this study, we used daily evaporation values  
108 calculated from measured latent heat fluxes corrected for the observed site-specific energy budget closure gap. In general,  
109 from 10 (Hetzdorf) up to 23 (Tharandt) years of continuous time-series are available.

110 The Grillenburg site (DE-Gri, the sensor height is 3 m above the ground) is a permanent and extensively managed (one to three  
111 cuts per year) flat-terrain grassland (mesophytic hay meadow). Regular mowing usually takes place in June and September. In  
112 the case of three cuts per year, the second one is usually done in July. Typical plant species include couch grass (*Elymus*  
113 *repens*), meadow foxtail (*Alopecurus pratensis*), common yarrow (*Achillea millefolium*), common sorrel (*Rumex acetosa*) and  
114 white clover (*Trifolium repens*). The area is generally used for forage and rarely for pasture. Vegetation height is measured  
115 once per week, with the lowest values (5-10 cm) measured at the beginning of growing season or after cutting and highest  
116 values (typically 30-40 cm, maximum 90 cm) in the summer before cutting. Although the LAI was only occasionally measured,  
117 the significant correlation between vegetation height and LAI made it possible to interpolate the annual range. Therefore, the  
118 range of LAI was estimated between 0.25 m<sup>2</sup> m<sup>-2</sup> and 5 m<sup>2</sup> m<sup>-2</sup> in the yearly course. The topography around the site promotes  
119 cold air deposition, thus daily minima of air temperature are often much lower than at the other sites. The site is mainly  
120 characterized by gleysol soil that contains silty loam, loam, and loamy silt as soil textures.

Отформатировано: Шрифт: (по умолчанию) Times New Roman, не полужирный, курсив, Цвет шрифта: Авто, Узор: Нет

Отформатировано: Шрифт: (по умолчанию) Times New Roman, 10 пт, курсив, Цвет шрифта: Авто, Узор: Нет

Отформатировано: Шрифт: (по умолчанию) Times New Roman, курсив, Цвет шрифта: Авто, Узор: Нет

Отформатировано: Шрифт: (по умолчанию) Times New Roman, 10 пт, курсив, Цвет шрифта: Авто, Узор: Нет

Отформатировано: Шрифт: (по умолчанию) Times New Roman, 10 пт, курсив, Цвет шрифта: Авто, Узор: Нет

121 The Klingenberg site (DE-Kli, the sensor height is 3.5 m above the ground) is an intensively farmed arable land located 4 km  
122 south from the Tharandt forest (Fig. 1). This site is characterized by annual and inter-annual crop rotation of rapeseed (*Brassica*  
123 *napus*), winter wheat (*Triticum aestivum*), forage maize (*Zea mays*), spring barley (*Hordeum vulgare*) and winter barley  
124 (*Hordeum vulgare*) with occasional intercropping. As a result, plant cover, vegetation height, LAI and rooting depth varied

Отформатировано: Шрифт: курсив

Отформатировано: Шрифт: курсив

Отформатировано: Шрифт: курсив

Отформатировано: Шрифт: курсив

Отформатировано: Шрифт: курсив

125 greatly across time periods, i.e. measured annual maximum canopy height values vary between 0.7 m and 2.2 m and LAI could  
126 reach up to 6 m<sup>2</sup> m<sup>-2</sup>. Soil properties and runoff behaviour are strongly influenced by tillage and fertilizer application.  
127 According to the (Ad-hoc-AG Boden, 2005), the soil was classified as gleysol and has a clay or loam texture.

128 The Hetzdorf site (DE-Hzd, the sensor height is 5 m (2010-2017), 11.5 m (2017-2021) and 17.5 m (since 2021) above the  
129 ground) is a young oak (*Quercus robur*) forest planted after the Kyrill storm in 2007, which caused severe windthrow (40 ha)  
130 in an old Norway spruce (*Picea abies*) forest. This site has a moderate slope to the North and a main wind direction to the  
131 South due to a gap in the surrounding old spruce forest. The young oak stand is approximately 8-10 m high (2021) and enclosed  
132 by spruce forest (up to 30 m height). Due to the high amount of deadwood and the young oak plantation until 2017 this  
133 ecosystem was a net CO<sub>2</sub> source, but since 2018 it already acts as a moderate CO<sub>2</sub> sink (Drought 2018 Team and COS  
134 Ecosystem Thematic Centre, 2020; Warm Winter 2020 Team and COS Ecosystem Thematic Centre, 2022). As a young  
135 growing site, LAI varies dynamically from year to year and was only measured sporadically. The site is dominated by  
136 pseudogley soil with a silt and silty loam texture.

137 The Tharandt site (DE-Tha, the sensor height is 42 m above the ground) is a 120-year-old mixed conifer forest with a mean  
138 canopy height of 30 m, consisting mainly of Norway Spruce (*Picea abies*, 80 %), European larch (*Larix decidua*, 18%), and  
139 various other evergreen and deciduous tree species (2 %) such as Scots pine (*Pinus sylvestris*), ~~Silver-silver~~ birch (*Betula*  
140 *pendula*) and ~~Mountain-mountain~~ ash (*Sorbus aucuparia*). Root depth amounted between 30 cm and 40 cm, relative to the  
141 predominant Spruce tree. The forest was thinned five times (1983, 1988, 2002, 2011 and 2016) and European beech (*Fagus*  
142 *sylvatica*) and Silver fir were planted in the understorey in 1995 and 2017, respectively. The site has silty podzol soils with  
143 relatively high stone content (10-20 %). These soils were developed from a periglacial sediment consisting of debris from  
144 rhyolite and loess and are very heterogeneous.

145 The Oberbaerenburg site (DE-Obe, the sensor height is 30 m above the ground) is an 80-year-old dense evergreen forest 15-  
146 17 m height with predominantly Norway spruce trees (*Picea abies*). In contrast to the other sites, this site is located much  
147 higher (734 m a.s.l.) with a prevailing NW wind direction and mean temperature and precipitation of 6.9°C and 960 mm,  
148 respectively. Spruce density has been thinned over the years (e.g., 1057 trees ha<sup>-1</sup> in 1994, 987 trees/ha in 2000, 884 trees ha<sup>-1</sup>  
149 in 2005, and 846 trees ha<sup>-1</sup> in 2011). However, this has had little effect on the site characteristics. The soil is characterized as  
150 podzol and has a sandy texture with high stone content (20-40 %).

151 According to on-site measurements, the groundwater tables for all sites are at least 3 m deep, thus is assumed, that there is  
152 no significant influence groundwater on the water demand for the evaporation.

153 Due to the principles of eddy-covariance measurements, the observed fluxes refer to a certain footprint that varies depending  
154 on wind speed, wind direction and atmospheric stability. Moreover, it is also affected by the height of measurement and the

Отформатировано: Шрифт: курсив

Отформатировано: Шрифт: курсив

Отформатировано: Шрифт: курсив

Отформатировано: Шрифт: курсив

Отформатировано: Шрифт: курсив

Отформатировано: Шрифт: курсив

Отформатировано: Шрифт: (по умолчанию) Times New Roman, 10 пт, курсив, Цвет шрифта: Авто, Узор: Нет

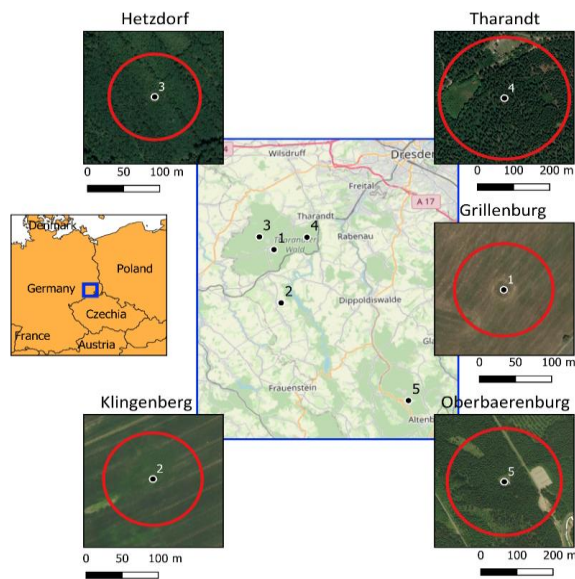
Отформатировано: Шрифт: курсив

Отформатировано: Шрифт: курсив

Отформатировано: надстрочные

155 surface roughness. According to long-term micro-meteorological measurements around the study sites, it was found that in  
 156 relation to predominant weather conditions the area of the highest flux density of the eddy-covariance signal (90 %) was within  
 157 a radius of 120-380 m. The values differ significantly among sites, but not greatly between wind directions (< 10 %). Thus,  
 158 equidistance footprints for each station (red circles on Fig. 1, shape files can be found in Supplementary) were assigned as  
 159 mean values from all wind directions. These values are further used in the simulations in model frameworks.

160 Selected daily evaporation data and other climatological variables can be found in the Supplementary.



161

162 **Figure 1. Location of chosen FLUXNET sites. Red circles represent footprints for each tower. OpenSteet Maps (Planet dump**  
 163 **retrieved from <https://planet.osm.org>) and Bing Satellite images (BingTM Maps tiles, 2020) are used as a background.**

164

**Table 1. Short summary on the chosen FLUXNET sites.**

ID	Site name	Latitude	Longitude	Available data	Footprint, m	Dominant soil type	Land cover type
1	Grillenburg	50.950	13.513	2003-2020	135	gleysol	Permanent grassland
2	Klingenberg	50.893	13.522	2005-2020	135	gleysol	Agriculture (with crop rotation)
3	Hetzdorf	50.9641	13.490	2010-2020	125	pseudogley	Young oak forest (after storm)

4	Tharandt	50.963	13.565	1997-2020	360	podzol	Old spruce forest
5	Oberbaerenburg	50.787	13.721	2008-2020	350	podzol	Spruce forest

165 **2.2 BROOK90 model**

166 BROOK90 (Federer et al., 2003) is a 1D process-oriented model for simulation of vertical water fluxes in soil-plant-atmosphere  
167 systems. Precipitation input (snow or rain) first goes through the canopy, where it could be intercepted and then evaporated.  
168 The portion, which reaches ground level, could be infiltrated, frozen, evaporated, converted to surface flow, percolated or  
169 stored as soil moisture. Infiltrated water follows a top-down approach as a macropore bypass and matrix flow. The soil column  
170 has groundwater, seepage and downslope outflow. Finally, soil water storage is used for evaporation and transpiration. The  
171 model has more than 100 physically-based input parameters, but typically most are straightforward and can be set easily (as  
172 location or slope). As the study mainly reflects evaporation, this part of the model is described in more detail.

173 The model uses a two-layer version of Penman-Monteith (PM) equation by Shuttleworth-Wallace (SW) (Shuttleworth and  
174 Wallace, 1985) to estimate the potential evaporation (PE) separately for canopy and soil surface accounting for the surface  
175 energy budget and the gradient for the sensible heat flux respectively. Canopy-dependent PE consists of evaporation of  
176 intercepted snow and rain and plant transpiration. It is defined as the maximum evaporation that would occur from a given  
177 land surface under given weather conditions if all plant and soil surfaces were externally wetted. Surface-dependent PE  
178 includes evaporation from soil and snow surfaces. It is defined as the maximum evaporation that would occur from a given  
179 land surface under given weather conditions if plant surfaces were externally dry and soil water was at field capacity. The SW  
180 method considers multiple resistances like the above canopy, within canopy from canopy and ground, canopy surface, vapour  
181 movement in soil. They are applied in the standard PM equation, thus giving separate estimates of all five components of PE.  
182 It should be noticed, as BROOK90 distinguishes between soil and plant evaporation, only one canopy process and one ground  
183 process can occur at a given timestep. Subsequently, actual evaporation (E) is based on the water availability in the system  
184 (within the canopy, on the soil and within the soil matrix). Daily evaporation rates are calculated as a weighted sum of the  
185 daytime and night-time values (based on the sunshine duration); however, interception could be estimated at a higher frequency  
186 (hourly).

187 Originally, the model was written in FORTRAN programming language, here we used an R ‘line-by-line’ direct translated  
188 version (Kronenberg and Oehlschlagel, 2019).

189 **2.3 Model frameworks and parameterization schemesschemes**

190 In the study, four different scale-dependent setups for the BROOK90 setupsmodel are used to simulate evaporation and its  
191 components, ~~with the BROOK90 model as the main core~~: Global BROOK90, EXTRUSO, BROOK90 with manual  
192 parameterization and calibrated BROOK90. To parameterize the model for global, regional and local scale different

193 topography, soil and land cover datasets were utilized. Most of the model's physical parameters are either default and thus  
194 fixed by the model developer or valid for whole model region (i.e. average duration of rain precipitation per month). Variable  
195 site-specific parameters (around 40 depending on the setup) and their values for all tested frameworks are listed in Appendix  
196 C (Table C1).

### 197 2.3.1. Global BROOK90 (GBR90)

198 The Global BROOK90 (GBR90) framework incorporates open-source global datasets for parameterization and forcing of the  
199 model using an R-package (Vorobevskii et al., 2020). The main feature of the package is wrapping of the modelling process  
200 in a fully automatic mode based only on the location and time-interval input. The input area of interest is divided in a regular  
201 50x50 m grid, and then hydro response units (HRU) are identified based on the unique combinations of land cover, soil  
202 characteristics, and topography (aspect and slope). GBR90 provides fixed parameter sets for 20 land cover types based of  
203 Copernicus Global Land Cover 100 m (Buchhorn et al., 2020): closed and opened forest (evergreen/deciduous, needle/broad  
204 leaf or mixed, and unknown), shrubs, herbaceous vegetation, moss and lichen, bare/sparse vegetation, cultivated and  
205 managed vegetation, urban territories and snow/ice. Additionally, Leaf Area Index (LAI) and tall canopy height  
206 parameters were assigned using MODIS 8-day composite dataset with 500 meter resolution (Myneni et al., 2015) and Global  
207 Forest Canopy Height with 30 m resolution (Potapov et al., 2021) respectively. The SoilGrids250 dataset (Hengl et al., 2017)  
208 provides global information on standard soil properties with 250 m resolution. Number of soil layers, stone fracture and profile  
209 depth parameters are directly derived from this dataset, while soil hydraulic parameters are assigned from the standard model  
210 developer's sets based on the derived USDS soil texture class. Amazon Web Service Terrain Tiles (Mapzen Data Products,  
211 2020) are used as provider for the global digital elevation model data (SRTM30 in case of Saxony). The model is applied  
212 separately to each HRU and an area-weighted mean is calculated. A more detailed description of the framework is presented  
213 in (Vorobevskii et al., 2020).

### 214 2.3.2. EXTRUSO (EXTR)

215 The EXTRUSO (EXTR) is a semi-automatic framework for spatial water balance simulations on a regional scale (up  
216 to now only unlimited to the domain of Saxony, Germany) and is distributed via R-package (Luong et al., 2020). The HRU  
217 subset is also based on the overlay of soil and land cover types derived from the regional datasets. Due to specifics of these  
218 datasets (polygons rather than regular grid rasters) HRUs do not have regular dimensions. The framework has fixed  
219 parameterization for 5 land cover types (agriculture/cultivated land, deciduous forest, evergreen forest, grassland/meadows,  
220 urban/other territories). They are assigned according to European land cover map CORINE 2012 (European Environment  
221 Agency, 2020) with 100 m resolution (some vegetation types from the map are generalized). Soil parameters are assigned  
222 similarly to GBR90, but using Saxon soil map BodenKarte50 (Sächsisches Landesamt für Umwelt, Landwirtschaft und  
223 Geologie, 2020) with 50 m resolution. The 10 m digital elevation model (Staatsbetrieb Geobasisinformation und Vermessung

Отформатировано: Шрифт: не полужирный

Отформатировано: Заголовок 3, интервал Перед: 0 пт, после: 0 пт

Отформатировано: английский (Соединенное Королевство)

Отформатировано: английский (Соединенное Королевство)

Отформатировано: английский (Соединенное Королевство)

Отформатировано: Шрифт: Times New Roman, 10 пт, Цвет шрифта: Авто

Отформатировано: английский (Соединенное Королевство)

Отформатировано: английский (Соединенное Королевство)

Отформатировано: английский (Соединенное Королевство)

Отформатировано: английский (Соединенное Королевство)

Отформатировано: английский (Соединенное Королевство)

Отформатировано: английский (Соединенное Королевство)

Отформатировано: Шрифт: не полужирный

Отформатировано: английский (Соединенное Королевство)

Отформатировано: английский (Соединенное Королевство)

Отформатировано: английский (Соединенное Королевство)

Отформатировано: английский (Соединенное Королевство)

Отформатировано: немецкий (Германия)

Отформатировано: немецкий (Германия)

Отформатировано: немецкий (Германия)



224 [Sachsen, 2020](#)) is used for slope and aspect estimates. As in GBR90, BROOK90 is run for each HRU and an area-weighted  
225 mean is stored. A full description of the framework is available in [\(Luong et al., 2020\)](#).

### 226 2.3.3. BROOK90 (BR90) with “expert-knowledge” parameterization

227 Finally, we made a setup using the original BROOK90 model (BR90) with manual parameterization based on field  
228 measurements. These include long-term observations of the different canopy parameters conducted on the chosen FLUXNET  
229 sites (height, LAI, conductivity, albedo), soil profile data (soil texture, depth, stone fracture) and expert knowledge (i.e.  
230 interception parameters).

### 231 2.3.3.4. Calibrated BROOK90 (CBR90) as a benchmark

232 The calibrated BROOK90 (CBR90) serves as a benchmark for all other runs. For the calibration of BROOK90, we choose a  
233 multi-objective optimizer recently developed for the calibration of hydrological models. The algorithm is a hybrid of the MEAS  
234 algorithm (Efstratiadis and Koutsoyiannis, 2005), which uses the method of directional search based on the simplexes of the  
235 objective space and the epsilon-NSGA-II algorithm with the method of classification of the parameter vectors archiving  
236 management by epsilon-dominance (Reed and Devireddy, 2004). A Pareto-optimal solution was used to address two issues.  
237 First, as most of total annual evaporation occurs in the vegetation period, it makes sense to separate this period as  
238 the contribution of the winter months should have lesser ‘weight’ during model fitting. Second we tried to account for possible  
239 systematic errors of eddy-covariance measurements themselves, which could vary significantly depending on the season  
240 (Hollinger and Richardson, 2005; Twine et al., 2000; Widmoser and Michel, 2021). Therefore, the Pareto front could help to  
241 choose an optimal parameter set, namely enhancing winter month performance with insignificant loss of performance in  
242 vegetation period).

243 Here, we performed calibration and validation with a 70 % – 30 % data split focusing on maximising daily KGE values for  
244 total evaporation for the growing season (March-October) and the winter period (November-February). The initial parameter  
245 sets were set by “expert-knowledge”. For the calibration we initially took the ‘location’ parameters within a  
246 physically meaningful range, which are recommended by the developer and other researchers as the most sensible (Groh et al.,  
247 2013; Habel et al., 2021; Schwärzel et al., 2009; Vilhar, 2016). After the manual sensitivity analysis conducted using the given  
248 site-specific data, 21 parameters were chosen. In general, these include albedo, vegetation and flow characteristics.  
249 Meteorological forcing was derived from in-situ measurements. The total number of trials was limited to 1000 model runs,  
250 which was sufficient to achieve stable performances for all three optimization functions.

251 Results of the calibration and validation are presented in Table 2. A complete list of chosen parameters with given ranges and  
252 a graphical overview of the resulting Pareto fronts for each site are provided in Appendix C (Tables C1 and C2). The raw  
253 outputs of calibration results for all trials with optimized parameters can be found in the Supplementary. It can be stated that

Отформатировано: английский (Соединенное  
Королевство)

254 [calibration and validation showed satisfactory results for the vegetation period even on a daily scale, while the results for the](#)  
255 [winter time were poor at most sites \(more in detail in Sect. 5.2 and 5.3\).](#)

256 **Table 2. Daily Kling-Gupta-Efficiency for BROOK90 calibration and validation.**

ID	Site name	KGE (Vegetation period)		KGE (Winter period)	
		Calibration	Validation	Calibration	Validation
1	Grillenburg	0.89	0.81	0.49	0.44
2	Klingenberg	0.72	0.67	0.19	-0.03
3	Hetzdorf	0.82	0.75	0.30	0.17
4	Tharandt	0.72	0.69	0.26	0.14
5	Oberbaarenburg	0.72	0.61	0.02	-0.94

#### 257 2.2.4 Climate data Meteorological forcings

258 We have chosen ERA5 (Copernicus Climate Change Service (C3S): ERA5: Fifth generation of ECMWF atmospheric  
259 reanalyses of the global climate. ERA5 hourly data on single levels from 1979 to present., 2020), RaKliDa (Kronenberg and  
260 Bernhofer, 2015) and in-situ station measurements to represent the global, regional, and local scales, respectively, as  
261 meteorological forcing for the [BROOK90 frameworks \(see Sect. 3.1\) model](#). The list of standard climatological variables  
262 required to run BROOK90 consists of minimum and maximum 2 m air temperature, mean 10 m wind speed, solar radiation  
263 on the horizontal surface, vapour pressure, and precipitation. Typically, daily data is required; however, if available, sub-daily  
264 precipitation data is more favourable.

265 The ERA5 is a global climate reanalysis dataset from Copernicus and European Centre for Medium-Range Weather Forecasts,  
266 available from 1950 to near real time at hourly resolution. It was derived using data assimilation principles by combining a  
267 global physical model of the atmosphere and observations from around the world. The original model resolution is 0.28125°,  
268 which corresponds to about 31\* $\times$ 20 km rectangle in the area of interest. For the present study, data from the nearest to each  
269 site ERA5 grid was downloaded and processed by aggregating hourly to daily values.

270 RaKliDa is an open-source daily climatological dataset covering the south-eastern part of Germany (namely Saxony, Saxony-  
271 Anhalt and Thuringia) with a time span of 1961-2020. The original station data from the German Meteorological Service and  
272 the Czech Hydrological Meteorological Institute are first corrected for wind errors (Richter, 1995) and then interpolated on a  
273 1x1 km grid using the Kriging indicator (Wackernagel, 2003). This approach is intended to reflect the orographic influence of  
274 downwind and upwind effects and to account for convective and small-scale precipitation events. As with ERA5, the nearest  
275 grid to each tower grid was used.

276 Daily meteorological data was taken from standard climate stations located in close proximity to the eddy-covariance towers.  
 277 Exception is the wind speed, which is measured on the same height with eddy-covariance. In addition, the available net  
 278 radiation was assimilated above the canopy. Prior data analysis revealed up to 15 % of missing values (depending on location  
 279 and variables). Since these values are generally not drastic, the majority of the missing parts fall within the model “warm-up”  
 280 period, and the variance of the most problematic variable (wind speed) within a site is not very high; it was decided to fill the  
 281 gaps with simple monthly averages.

282 All of the inputs required by BROOK90 are directly available in all three data sets, except for the vapour pressure, which was  
 283 calculated using dew temperature data (Murray, 1967) for ERA5 and mean daily temperature with relative humidity for two  
 284 others (Magnus formula).

285 The meteorological data prepared for BROOK90 can be found in Supplementary. A graphical overview of the differences  
 286 between three data sets is presented in Appendix A ~~and will be discussed later on.~~

287 Of the six input meteorological variables, net solar radiation and precipitation have the biggest influence on evaporation.  
 288 Global radiation in the gridded datasets showed minor but systematic overestimation compared to measurements on the mean  
 289 daily scale (around 1 MJ\*m<sup>-2</sup>\*day<sup>-1</sup> in winter and 2-3 MJ\*m<sup>-2</sup>\*day<sup>-1</sup> in summer months). However, summer variations (peaks  
 290 and minimums) are underestimated probably due to cloud coverage problems in ERA5 and RaKliDa. Precipitation showed a  
 291 much larger and non-systematic difference between the three datasets. In general, higher mean daily precipitation was  
 292 measured from September to March in Grillenburg, Hetzdorf and Tharandt (0.5-2 mm\*day<sup>-1</sup>). However, when looking at the  
 293 BIAS values (Table 3), a negative BIAS is typical for both datasets (except Klingenberg for both and Tharandt for RaKliDa).  
 294 The behaviour of the vegetation and winter periods separately follows the annual BIAS. Temperature and available vapour  
 295 pressure appear to be consistent, with 1-3 degree and 0.01-0.03 kPa respectively variation from measurements in the summer  
 296 months. The exception is Oberbaerenburg, where the maximum temperature and available vapour pressure from ERA5 and  
 297 RaKliDa have higher deviations, probably due to neglecting higher altitude in the datasets. Finally, wind speed possesses a  
 298 systematic positive biasBIAS (1-2 m\*s<sup>-1</sup>) for all months, except for ERA5 in forests and Klingenberg.

299 Table 3. Precipitation BIAS (to in-situ measurements).

Site name	Meteo Dataset	Year	Vegetation period	Winter period
Grillenburg	ERA5	0.91	0.95	0.83
Klingenberg		1.05	1.05	1.05
Hetzdorf		0.92	0.96	0.85
Tharandt		0.96	1.01	0.85
Oberbaerenburg		0.76	0.85	0.59
Grillenburg	RaKliDa	0.88	0.92	0.8

<u>Klingenberg</u>		<u>1.04</u>	<u>1.02</u>	<u>1.08</u>
<u>Hetzdorf</u>		<u>0.88</u>	<u>0.93</u>	<u>0.77</u>
<u>Tharandt</u>		<u>1.15</u>	<u>1.16</u>	<u>1.12</u>
<u>Oberbaerenburg</u>		<u>0.71</u>	<u>0.78</u>	<u>0.57</u>

### 3.2.2.5. Evaluation of parameterization and forcings combinations

To assess the ~~uncertainty~~ ~~sensitivity~~ ~~sensitivity~~ of the BROOK90 ~~setups to different parameter and meteorological inputs~~ with regard to the evaporation ~~components~~ ~~simulations~~, we propose to create different combinations of the framework's parameterizations from global, regional and, local schemes and meteorological inputs from global, regional and local datasets (Fig. 2). Additionally, we tested the sensitivity of the setups to the temporal resolution of the forcing data (hourly and daily for ERA5). ~~Our main hypothesis is that the goodness of fit of the setups decreases from global to local scale (for both parameterization and forcing). We were particularly interested in testing the local-global combinations, i.e. BROOK90 with ERA5 forcing and Global BROOK90 with station data forcing.~~

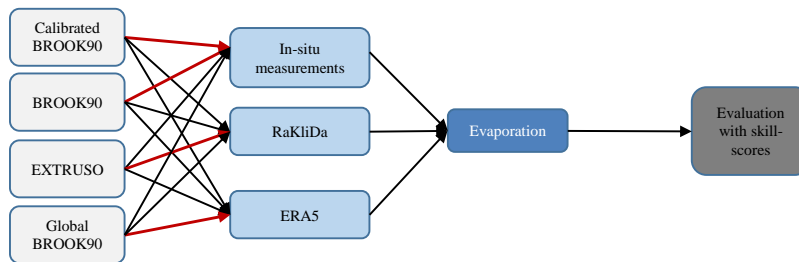


Figure 2. Principal scheme of the framework's mixture. Red arrows represent the original "parameter set – meteorological forcing" combination.

From the model runs, we extracted total evaporation and its five components: transpiration, evaporation of intercepted snow and rain, evaporation from soil, and snow evaporation. These results were evaluated on daily and monthly scales for the whole year and separately for the winter and vegetation periods using the following performance metrics: Mean Absolute Error, Nash-Sutcliffe Efficiency (NSE) (Nash and Sutcliffe, 1970) and Kling-Gupta Efficiency (KGE) (Gupta et al., 2009). The last one can be decomposed into three main components important to assess process dynamics: correlation, ~~bias~~BIAS, and variability errors. ~~Since all the proposed metrics are well-known, we omit~~The formulas ~~and optimal ranges for each performance metrics in main-text and are~~ listed them in Appendix B.

Additionally, to test the uncertainty of the obtained performance, a small data resampling experiment was designed (here only for the daily KGE values). ~~It helps to show the possible performance spread due to general time-series shortage and occurrence of some extreme years (e.g. like wet 2003 and 2012 or dry 2018 and 2019).~~ Thus, for each station we calculated multiple KGE

321 values with reduced time-series length by randomly (1000 samples with replacement) throwing away 3 years of data (same for  
322 all cross-combinations). Obtained values serve to assess the possible KGE spread for each framework and meteorological  
323 dataset.

## 324 2.6 FAO grass-reference evaporation

325 ~~The FAO approach was chosen to compare the relative complexity for the comparison with the BROOK90 model. Both~~  
326 ~~approaches of them with other one, but in the same time remain on the same methodological background of are based on the~~  
327 ~~Penman-Monteith equation, the FAO approach was chosen. The FAO approach method is considered as a state-of-the-art for~~  
328 ~~grass-reference evapotranspiration estimations (Paredes et al., 2020; Sentelhas et al., 2010). Potential daily evaporation values~~  
329 ~~are obtained on the basis of a simplified Penman-Monteith approach (facilitations concern aerodynamic and surface~~  
330 ~~resistances calculations) with the radiation (shortwave and longwave), air temperature, wind speed and humidity as the input~~  
331 ~~data (Allen et al., 1998). The approach simplifications are concerning the aerodynamic and surface resistances calculations.~~

## 332 4-3 Results

### 333 4.3.1. Daily and monthly total evaporation

334 ~~Before discussing the performance criteria~~At first, a visual analysis of the modelled evaporation was performed. Therefore,  
335 daily (for 2020) and monthly (for the whole period with available measurements) time-series (Appendix D), monthly quantile-  
336 quantile (Fig. 3) and mean monthly (Fig. 4) plots were analysed.

337 Daily evaporation of 0-0.5 mm in winter and up to 6-7 mm in summer months (with a maximum of about 10 mm) was found  
338 for the Grillenburg's grassland. All model setups showed similarly low values in November-February. The growing period  
339 (March-May) was represented with a delay of 3-4 weeks for GBR90 and EXTR and 2-3 weeks for BR90. Calibration helped  
340 to eliminate this time shift on a monthly scale, however at the same time enhancing the unreasonably high variability on a  
341 daily scale. During the summer months (June-August), the frameworks suffered ~~from the systematic increasing overestimation~~  
342 ~~of variance ratio and underestimation of the mean values~~systematic underestimation, which ~~got worse~~is especially noticeable  
343 ~~within~~ the higher ~~evaporation values range~~values. Moreover, monthly maximum values vary from year to year due to  
344 differences in the timing of grass cuts. Evaporation in autumn is well captured but advanced by 2-3 weeks in EXTR and BR90.  
345 Finally, the difference between meteorological datasets is only noticeable in the summer months.

346 In Klingenberg's crop field, evaporation of 0-1 mm in winter and 4-6 mm in summer months (with maximum around 9 mm)  
347 is usually observed. In most of the years, all model setups showed a similar small overestimation in November-January. It was  
348 relatively difficult to achieve ~~a good model fit~~good timing regarding the timing of the growing and harvesting periods for the  
349 ~~vegetation period~~even on a monthly scale. Since the ~~growing and harvest~~both periods of the various crops differ by up to two

350 months and the annual rotation with clear cuts are irregular. The growing period (February-May) had in general a delay of 2-  
351 6 weeks. Here CBR90 shows higher daily evaporation values, thus fitting ~~good~~-low BIAS, while the variance ratio stays  
352 underestimated. In contrast with the grassland site, summer months (June-August) did not depict a high ~~bias~~BIAS, the main  
353 ~~uncertainty-problem~~ ~~lies~~-appears in a considerable scattering ~~due to poor correlation~~, which is higher in the middle part of QQ-  
354 plot. Furthermore, the different setups showed different peak values in the summer months, BR90 matched observations in  
355 June, while GBR90 and EXTR showed the maximum in July. Finally, in autumn, none of the setups provided satisfactory  
356 results, namely both over- and underestimations, especially in September and October. Again, based on the meteorological  
357 datasets, the variability of the model performance is visible only in the summer months.

358 For the Hetzdorf deciduous broadleaf forest, typical values of winter and summer evaporation are 0-1 mm and 3-5 mm (with  
359 maximum around 8.5 mm), respectively. All model setups showed small amounts of evaporation in winter with a low  
360 ~~bias~~BIAS, but also low correlation. The main leaf development period (March-May) was represented well by GBR90, with a  
361 2-3 weeks' time lag in April for EXTR and BR90. In the summer months (mostly in June and July) GBR90 and EXTR  
362 underestimated evaporation by 10 %, while 'expert knowledge' BR90 gave positive BIAS. It can be noticed on the monthly  
363 plots that as the forest keeps developing and growing intensively within the last 10 years, higher evaporation rates were  
364 observed from year to year. At the same time due to model parameter stationarity, BR90 shows closer to the observed  
365 evaporation values only in the last two years. The annual mean monthly peak (July) and leaf fall were well captured by all  
366 models. Here the variance ~~errors-ratio~~ reach ~~minimum~~-the closest to the optimum values in comparison to all the other sites.  
367 Only for the summer months, a rather small difference of about 10 mm per month between the meteorological forces could be  
368 captured.

369 In the evergreen coniferous forest of Tharandt, daily evaporation usually yields 0-0.3 mm in winter and 2-3 mm in summer  
370 (with maximum around 7 mm). All setups except CBR90 demonstrated a high BIAS for the seasons (15-20 mm per month),  
371 which is larger in winter, where daily peaks are sometimes as high as summer maximums. Moreover, the inter-annual  
372 variability appears to be highly overestimated as well. Like for the grassland, the model calibration reduced the mean error to  
373 optimum values, but the problem of daily peaks in winter remained unsolved. In contrast to the other sites, a noticeable  
374 difference between forcings can be observed (up to 10 % in the summer months) with the in-situ measurements delivering the  
375 highest evaporation amount.

376 The evergreen coniferous forest of Oberbaerenburg -normally has evaporation rates of 0-0.3 mm in winter and 2-3 mm in  
377 summer (with maximum around 8 mm). Evaporation here is 5-10% higher in the growing season than at the Tharandt site.  
378 Still, most of the setups (except in spring and CBR90) showed a positive BIAS, which is higher in winter and July. Similar to  
379 Tharandt, winter daily peaks sometimes exceeded summer extremes. Here, even the calibrated model did not demonstrate a  
380 good agreement in general and did not remove winter overestimations. Oberbaerenburg was the only site where the well-  
381 known European drought of 2018 is clearly visible on a monthly scale. The data shows around 30 % less evaporation in

382 summer months due to depletion of the soil water and overall precipitation deficit. However, most of the model setups did not  
 383 depict this effect properly. Finally, the spread between meteorological datasets here is not as broad as for the Tharandt site.

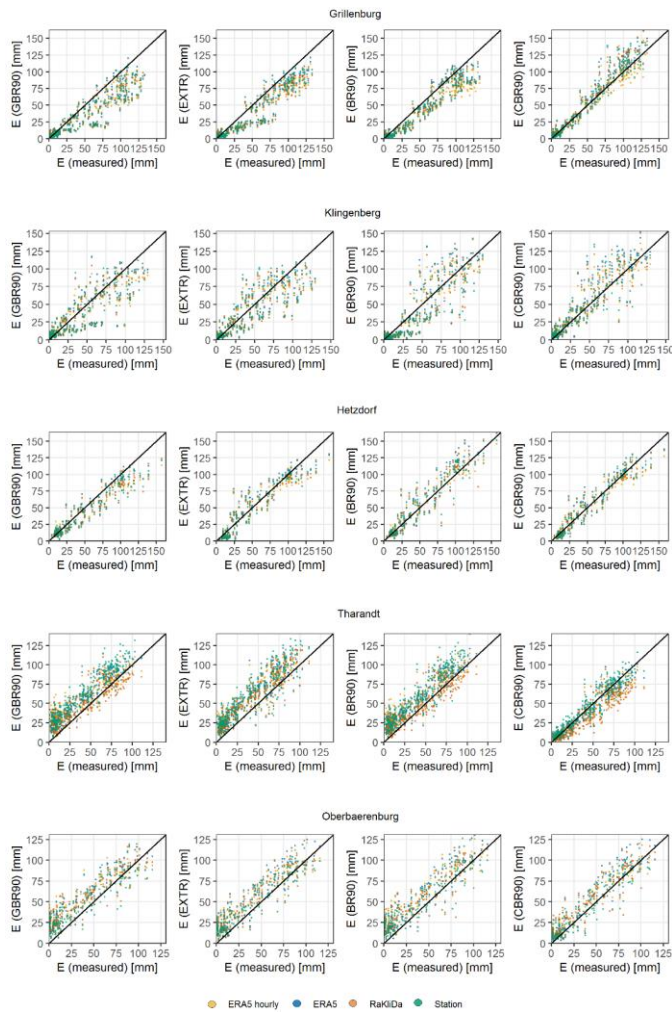


Figure 3. Observed and modelled monthly evaporation values for all setups.

384  
 385

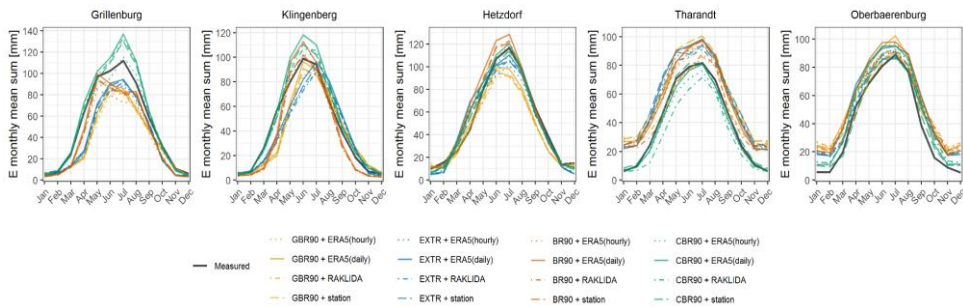


Figure 4. Observed and modelled monthly mean evaporation values for all setups.

386  
387

388 In Fig. 5, the daily KGE values are shown, while the monthly results and other criteria (NSE, MAE) are presented in Appendix  
 389 E. Based on KGE values, a good agreement was found between all model setups and observations for all the sites (Fig. 5). The  
 390 best agreement showed the combination “CBR90 + station data” (from 0.72 in Oberbaerenburg to 0.91 in Grillenburg) and the  
 391 worst “GBR90 + hourly ERA5” (from 0.36 in Grillenburg to 0.71 in Hetzdorf). On the monthly scale, all setups demonstrated  
 392 higher performance, which is approximately 5 % better than on the daily scale. The ~~Goodness-goodness-of-of-fit~~ in the  
 393 vegetation period was better and very similar to the whole year, while ~~the performance~~ in winter ~~time for all setups performed~~  
 394 ~~not so well was lower~~, resulting sometimes in negative KGE values (down to -0.6). Here BR90 and EXTR showed ~~distinctly~~  
 395 ~~worse poor outcomes-agreement with the observations~~ in the fields (Grillenburg and Klingenberg) and in the deciduous forest  
 396 (Hetzdorf) respectively.

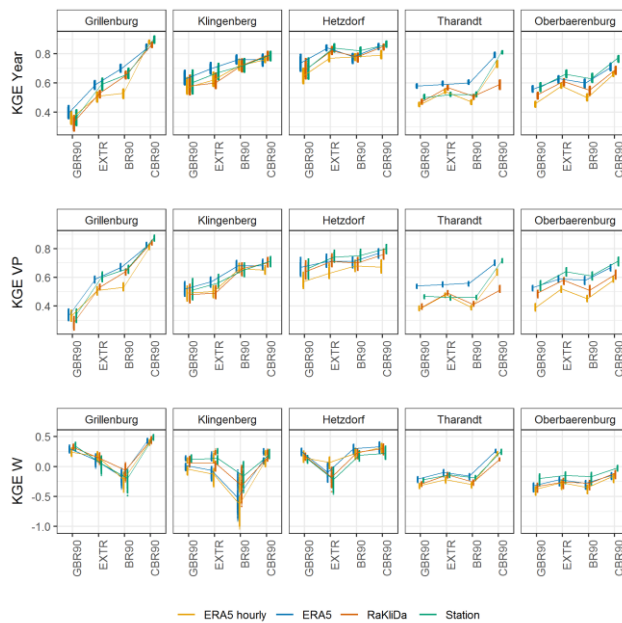
397 With a few exceptions, the best performance among the meteorological datasets was achieved for the station data and daily  
 398 ERA5. On average for all the five sites, in terms of KGE values, the spreads in the meteorological forcings yielded 0.09 0.1  
 399 (maximum of 0.17 showed BR90 for Grillenburg), while scattering in the parameterization schemes was much higher and  
 400 yielded 0.25 (with the maximum of 0.54 0.5 for Grillenburg and in-situ meteo data).

401 Finally, KGE spreads calculated for each combination from a resampled time-series are generally small. On the annual scale  
 402 and for the vegetation period, higher uncertainties of obtained KGE values were found in Grillenburg, Klingenberg and  
 403 Hetzdorf (10-15 % on average); while in Tharandt and Oberbaerenburg KGE deviations were low (around 5 %). For the winter  
 404 months, the spread possessed the same behaviour, but resulted in much higher values (up to 100%). Among all the frameworks,  
 405 GBR90 was associated with the largest uncertainty on the annual scale in almost all the cases, while it had the smallest spread  
 406 in the winter, where uncertainty of EXTR and BR90 dominated.



407 NSE values are in general similar to KGE, but slightly smaller, which range from -0.05 for GBR90 in Grillenburg and  
 408 Oberbaerenburg to 0.88 for CBR90 with station data. Mean average errors vary from 0.39 up to 0.98 mm\*day<sup>-1</sup> with the highest  
 409 values in evergreen forests for GBR90 and the lowest in Grillenburg for CBR90.

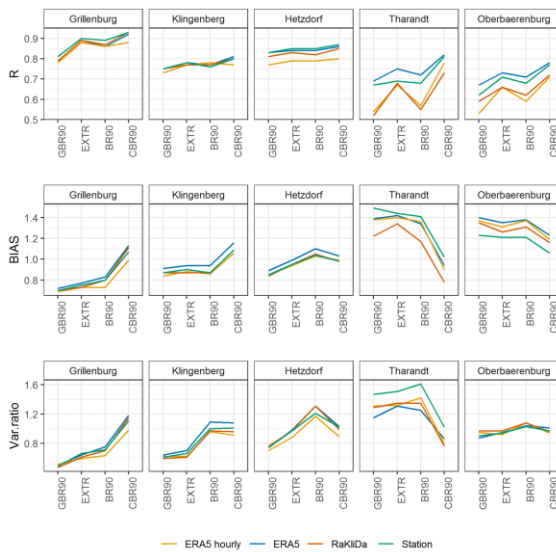
410 The hourly-resolved ERA5 data did not produce better results, showing the worst performance on the annual scale in most  
 411 cases.



412  
 413 **Figure 5. KGE values for daily evaporation: whole year, vegetation and winter periods. Vertical lines for each cross-combination**  
 414 **refer to bootstrapped KGEs.**

415 The major advantage of the KGE criteria is the possibility to obtain a deeper understanding of model uncertainty-performance  
 416 through its decomposition. A closer look at the KGE components (Fig. 6) reveals that correlation coefficients for the fields  
 417 (Grillenburg and Klingenberg) and deciduous forest (Hetzdorf) are relatively high for all model setups (0.75-0.95), and the  
 418 main problems occur in underestimation of the mean (0.7-0.8) and variability ratios (0.55-0.7) (except for BR90 in Hetzdorf).  
 419 In general, there are only small fluctuations between model forcings for these three sites. In evergreen forests, on the other  
 420 hand, the correlation showed much higher spread among both parameterizations and meteorological datasets (0.4-0.75).

421 Furthermore, bias-BIAS and variability ratios are, on possess on the other side, overestimated-significant positive deviations  
 422 from the optimal values (except variability in Oberbaerenburg), especially in Tharandt (up to 1.6). Overall, ERA5 and station  
 423 data perform better than others in most of the cases do. The hourly ERA5 forcing did not produce-show a noticeable difference  
 424 in evaporation bias-BIAS or variability, but reduced correlation in the forests (by 5-15 %). Finally, it could be noticed that in  
 425 comparison to the other setups, CBR90 bring bias-BIAS and variance ratio almost to one, but did not improve correlation for  
 426 all the sites (i.e. Hetzdorf).

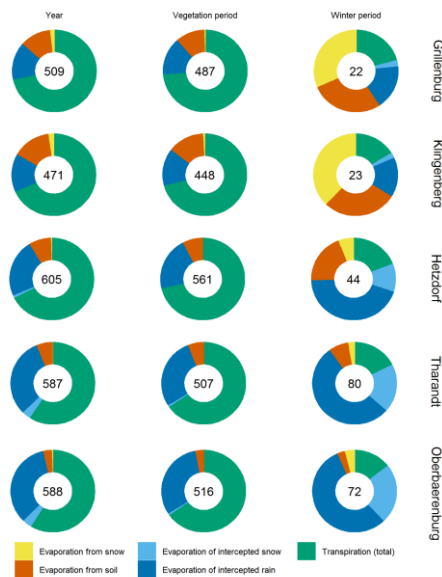


427  
 428 **Figure 6. Decomposition of KGE for daily evaporation for the whole year: correlation, BIAS and variance ratio**

429 **4.3.2. Evaporation components**

430 The 40-60 % partitioning between total flow and evaporation components in global terrestrial water balance (Müller Schmie  
 431 et al., 2016) also applies to the BROOK90 point simulations. With a variation in mean annual precipitation from 877 mm  
 432 (Klingenberg) to 1141 mm (Oberbaerenburg), measured mean annual evaporation varies from 476 mm (Tharandt) up to 625  
 433 (Hetzdorf) mm. This leads to measured E-P ratios of 0.41 to 0.65, with the lowest values observed in old spruce forest and the  
 434 highest in grassland and growing deciduous forest. Here, both the global and regional frameworks showed an overestimation  
 435 of the ratio for the evergreen forests (Tharandt and Oberbaerenburg) and an underestimation for the fields (Grillenburg and  
 436 Klingenberg) (could be found in Supplementary).

437 (Wei et al., 2017; Zhang et al., 2017) Overall, 60 % of annual global terrestrial evaporation consists of plant transpiration, 22  
 438 % of water attributes to evaporation from soil and snow and finally interception contributes up to 18 % (Wei et al., 2017). We  
 439 summarized the annual evaporation components (averaged from all tested model setups) are presented on (Fig. 7) of all tested  
 440 model setups. According to this figure, transpiration in fields and deciduous forest yields 68-73 %, and evergreen forest  
 441 transpires about 58-59 %. In Tharandt and Oberbaerenburg 31-35 % of precipitation goes to interception (mainly rain,  
 442 interception of snow is less than 2 %). In Grillenburg, Klingenberg and Hetzdorf evaporation of the intercepted precipitation  
 443 is lower and yields 14-23 %. Soil evaporation on the other side, is higher in the fields (11-15 %) and lower in forests (4-8 %).  
 444 Evaporation from snow is less than 2 % at all sites. The vegetation period spans 8 months in total and accounts for most of the  
 445 annual evaporation (85-95 %). Thus, the distribution of components is generally consistent with a slightly higher contribution  
 446 from transpiration. In winter, evaporation consists mainly of interception in forests and soil or snow evaporation of the fields.



447  
 448 **Figure 7. Mean annual and seasonal evaporation components averaged over all model setups. The numbers inside pie charts refer**  
 449 **to the mean evaporation sums per year or season.**

450 To get more insights on the possible setups' differences regarding the evaporation partitioning, we show "natural" model  
 451 parameterization and forcing combinations (Fig. 8). Only minor differences were observed in evergreen coniferous forests.  
 452 This mainly concerns intercepted rain. GBR90 with hourly ERA5 shows the largest amount (40-68 %) and CBR90 with station

453 data reduces interception up to 15-30 %, which is especially noticeable in Oberbaerenburg. At the other three sites, seasonality  
454 plays a bigger role in the redistribution of evaporation components. Indeed, in the fields, almost no interception was modelled  
455 in EXTR using RaKliDa and BR90 with station data in winter and early spring, and all evaporation in these months consists  
456 of snow and soil evaporation. Furthermore, the transpiration is dominant in summer and autumn times with sharper edges due  
457 to crop and grass cutting. In general, EXTR delivers more soil evaporation than other model setups, while GBR90 produces  
458 more rain interception. Slightly smoothed but similar results could be observed in the deciduous forest of Hetzdorf. Since  
459 the actual distribution of the components is unknown, we can only assume that CBR with in-situ meteorological data indicates  
460 conditions that are the closest to reality. Considering this, we can rank the goodness of the framework in the evaporation  
461 representation in the following order (best to worst by similarity to CBR90): BR90, EXTR, GBR90, which seems indeed  
462 logical.

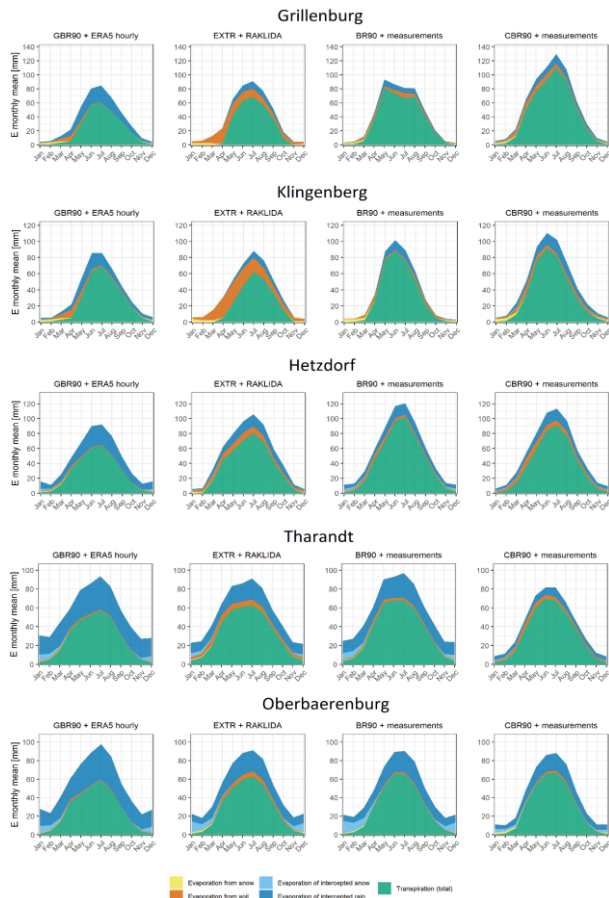


Figure 8. Modelled mean monthly evaporation components.

### 3.3 Grass-reference evaporation: comparison of BROOK90 and FAO model with measurements

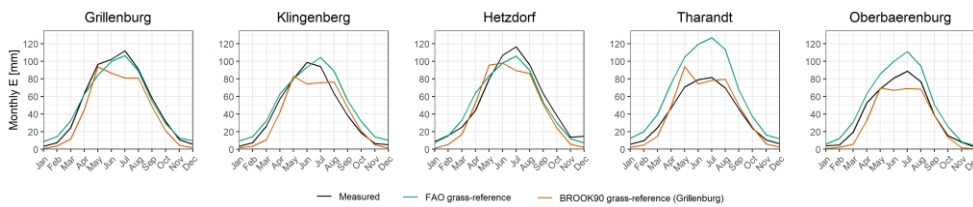
The Results of comparison the FAO “potential” and BROOK90 “actual” grass-reference evaporation output isare presented in Figure. 9. For that To simulate a BROOK90-based grass-reference evaporation, in the BROOK90 model the original site-specific vegetation parameters were replaced withby “grassland” onesparameters fromassumed at the Grillenburg manual

469 parameterization scheme site in the model. Station The meteorological input data was considered for both approaches remained  
470 site specific for both approaches.

471 The FAO estimations of the field sites (Grillenburg and Klingenberg) showed a good fit with the observed data. ~~;~~  
472 ~~except~~ Deviations are observed as a time lag of one+ month ~~in the autumn time~~ and minor overestimations of evaporation in  
473 winter time (5-10 mm per month). While the BROOK90 simulations possess a ~~noticeble~~ noticeable time lag of a 2-3 weeks in  
474 the spring periods ~~and~~. Also visible is an up to 20% underestimation ~~in the of~~ of evaporation in spring and summer months ~~up to~~  
475 ~~20%~~ is visible.;

476 Minor variances of around 10 mm per month between FAO and measured evaporation ~~could be seen~~ are observed in the  
477 ~~desiduous~~ deciduous forest of Hetzdorf. Namely there is a small overestimation in the spring period and an underestimation  
478 in summer months. The A“actual” grass-reference evaporation from BROOK90 ~~simulations~~, on the other hand was mainly  
479 lower ~~then~~ than the eddy-covariance measurements for all months, except for April and May.

480 In evergreen forests the FAO approach depicted considerably higher potential grass-reference evaporation than it was observed  
481 ~~throughout~~ throughout the whole year. These high evaporation estimates of up to 30-40% (July) are ~~but especially~~ very high  
482 in summer months ~~(up to 30-40% in July)~~. BROOK90 did not show such high systematic deviations from the observations in  
483 Tharandt ~~(except the for a peak in May)~~. While in Oberbaerenburg the simulated evaporation was systematically lower for  
484 all months ~~(and especially in summer time)~~.



485

486

**Figure 9. Observed and modelled monthly mean grass-reference evaporation.**

## 487 **5.4 Discussion**

### 488 **5.4.1. Role of the framework's spatial scale in parameterization and forcing**

489 The comparison of GBR, EXTR and BR90 frameworks showed how the model is sensible BROOK90 is to the  
490 spatial scale of the setup with regard to evaporation. Moreover, coupled with the fact that CBR90 showed significantly higher  
491 performance skill scores than the other setups for almost all the sites, it was indirectly confirmed indirectly that the

492 ~~model~~BROOK90 is more sensible to the scale of parameterization scheme rather than to the scale meteorological forcing.  
493 However, these conclusions need to be backed up with the assumption that both meteorological data and parameters used for  
494 each spatial scale come from state-of-the-art sources. Thus, they are both representative and possess the best quality (currently)  
495 for global, regional and local scales respectively.

496 The ~~A~~analysis of the parameters used in the study and their ranges revealed which groups of them ~~demonstrated~~possess the  
497 most noticeable influence on the accuracy of evaporation simulations and are at the same time affected by the scale of the  
498 model setup (Appendix C, Table C1).

499 At first, the plant leave's parameters must be highlighted, namely albedo, LAI and height, interception storages. Surface  
500 reflectivity with and without snow regulate the net radiation and thus directly affects potential evaporation. The values  
501 generally have a wide range 0.1-0.3 for vegetation and 0.2-0.9 for snow and their estimations are subject of high uncertainties  
502 (Alessandri et al., 2020; Myhre and Myhre, 2003; Page, 2003; Park and Park, 2016; Wang et al., 2017). For GBR90 and EXTR  
503 respectively~~Here, the~~albedo ~~was~~ere assigned by values taken from~~with~~ global and regional studies ~~for GBR90 and EXTR~~  
504 ~~respectively~~, while for BR90 measured values were used. Maximum LAI and its seasonal cycle are ~~probably~~probably the most  
505 ~~sensible~~sensible and uncertain parameters in the model regardless of the vegetation type, while plant height and its seasonality  
506 plays a greater role and is more uncertain for the short (~~grass and cropland~~), rather than in tall (~~forest~~)-canopies. These two  
507 parameters often control the ~~biggest~~largest portion of potential evaporation (~~controlling~~ transpiration and interception )as well  
508 as its partitioning (Hoek van Dijke et al., 2020; Wegehenkel and Gerke, 2013; Yan et al., 2012). ~~Here~~On the global scale  
509 ~~was~~both parameters are derived by ~~represented~~with remote sensing estimates, while on the regional and local scale~~use~~ fixed  
510 values from regional studies and expert knowledge ~~were taken, which~~ Therefore, at these scales the ~~simulations~~simulations apparently  
511 showed better results for the case-study. The interception storage and intercepted precipitation fraction are the key parameters  
512 for the correct estimation of interception amount (Wu et al., 2019). They are all plant-, season- and age-dependent, and possess  
513 a high variability, which makes its very challenging to generalize their values for the vegetation classes (Federer and Douglas,  
514 1983; Leaf and Brink, 1973; Pypker et al., 2005; Yang et al., 2019). In all frameworks they are set up as default or with expert  
515 knowledge. Nevertheless, only due to these ~~parameters~~parameters, the interception uncertainty could be as high as  $\pm 20$  mm  
516 per month, especially in forests.

517 The ~~S~~second group denotes to soil parameters. The ~~S~~soil structure, profile depth and ~~coarse~~coarse fragment's fraction directly  
518 determine the maximum water ~~storage~~storage capacity for ~~the~~a site. Here, the ~~parameter~~parameter scale plays a crucial role, since, the  
519 quality of available datasets decreases drastically from a local to a global scale due to ~~scarcity~~scarcity of soil profile data and  
520 very high heterogeneity of soils (Hengl et al., 2017)(REF). Soil hydraulic properties certainly ~~undoubtedly~~fully have a big influence  
521 on the water retention and holding capacity, controlling water ~~supply~~supply for the actual soil evaporation and transpiration  
522 (Carminati and Javaux, 2020; Lehmann et al., 2018; Verhoef and Egea, 2014). However, the scale uncertainty due to this  
523 parameter group is difficult to assess, since these parameters are assigned indirectly based on sand, silt and clay content for

524 each layer and fixed parameter set. Thus, the problem is narrowed to correct identification of the soil texture, which is still a  
525 very challenging task even for a regional scale (Hengl et al., 2017).

526 Significant difference in the model performance due to different meteorological input datasets was not evident for all setups  
527 and sites (ep-bootstrapped values on Fig. 5). Here, the spatial scale did not follow the main hypothesis, as the global dataset  
528 ERA5 was not the worst and in many cases outperformed in-situ meteorological data. It would appear, that the RaKliDa dataset  
529 with its 1 km spatial resolution could fit the eddy-covariance footprint at least as good as station data, however, it sometimes  
530 demonstrated the worst performance or close to hourly ERA5. This outcome contradicts with the generally accepted  
531 application of regional meteorological forcings to simulate evaporation in high resolution (Martens et al., 2018; Rudd  
532 and Kay, 2015; Wang et al., 2015; Zink et al., 2017). However, probably due to location peculiarities of the study sites, and  
533 good agreement of the global reanalysis with station data, regional dataset did not show a competitive performance.  
534 Namely, ERA5 showed slightly better precipitation BIAS values, than RaKliDa (Table: 3). Moreover, RaKliDa exhibits a  
535 systematic underestimation of the global radiation, especially in the summer months (Appendix A).

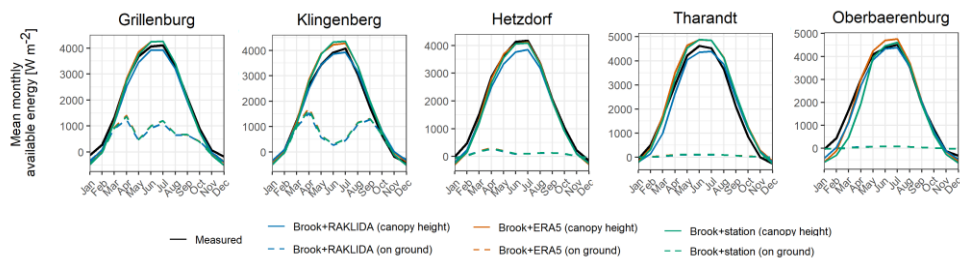
#### 536 5.4.2. Challenges in the model process representation

537 Although BROOK90 has a fairly good decent physically-based description-representation of the evaporation process, it shows  
538 some limitations as well. At first, BROOK90 treats the vegetation as a single layer (big-leaf). Thus, the complexity of canopy  
539 vertical structure is omitted, which can be insignificant for simple ecosystems like meadows or cropland, but  
540 can might play a big role in multi-layered vegetation (Bonan et al., 2021; Luo et al., 2018; Raupach and Finnigan,  
541 1988). For example, the lack of undergrowth representation could have a significant effect on the evaporation  
542 underestimation in forests with a dense floor like Hetzdorf. Additionally, there is no allowance for non-green leaves, which  
543 intercept precipitation and radiation, but in the meantime do not transpire. This process can play a role in deciduous forests  
544 like Hetzdorf in autumn and winter, as they generate too much transpiration. Furthermore, since the phenomenon of ground  
545 frost is not considered, soil evaporation is not limited on these days, which could lead to a substantial overestimation in  
546 winter. As canopy parameters are assumed constants, phenology or growth (e.g. crop rotation in Klingenberg and continuous  
547 forest growth in Hetzdorf) as well as drought affecting LAI (reduction due to prolonged water stress) are not considered in the  
548 model. Snowpack energy and evaporation modules suffer from overestimations in tall canopies, thus an arbitrary reduction  
549 factor is applied. Finally, albedo does not depend on solar elevation angle, canopy structure, or snow age. These limitations  
550 alone could have a substantial influence on total evaporation and its timing.

551 In addition, the PM equation uses vapour pressure deficit and net energy as the main factors to calculate potential evaporation.  
552 The first variable is derived directly from the daily input temperature and available vapour pressure using the Magnus equation  
553 and does not vary much between different methods (Lide, 2005). For net energy, the situation is different. The shortwave  
554 radiation is an input and its net value is controlled by the rather vague albedo, while the longwave radiation is estimated  
555 internally using the effective emissivity of the clear sky. Under these assumptions, the potential discrepancy uncertainty



556 between different formulas can be as high as 20-30  $W \cdot m^{-2}$ . After obtaining a persistent positive BIAS for evaporation in the  
 557 forests, we checked the energy balance of the model with in-situ measurements (Fig. 910). In fact, minor differences were  
 558 found for all input datasets. In the summer period, minor overestimation was found for ERA5 and station data in Grillenburg,  
 559 Klingenberg and Tharandt, and underestimates for RaKliDa in Hetzdorf and Tharandt. In winter (especially in December and  
 560 January), large relative underestimation was discovered in Grillenburg, Hetzdorf and Oberbaerenburg. Therefore, with a  
 561 negative amount of energy, BROOK90 still showed higher monthly evaporation than measured. Specifically, according to Fig.  
 562 8, 90 % of the actual evaporation in forests in winter consists of interception, and normally there is no absence of precipitation  
 563 input during this period. Because of the peculiarities of the PM approach, positive potential evaporation can be estimated with  
 564 negative net energy, positive vapour pressure deficit, and low estimated atmospheric and canopy resistances. Thus, as long as  
 565 vapour pressure deficit exists, the evaporation flux tries to fill the gradient.



566  
 567 **Figure 910.** Observed and modelled monthly mean net energy on canopy and ground level.

568 Finally, as it was found, the hourly-resolved ERA5-input precipitation data did not produce better results, showing the worst  
 569 performance (hourly ERA5 data) on the annual scale in most cases. There are few possible explanations for that. At first, due  
 570 to the shortcomings this brings up the question of reliability of the subdaily calculations in BROOK90 interception module,  
 571 which i.e. omits diurnal cycle of potential evaporation and consistently produce too much interception if hourly precipitation  
 572 input is used (Federer, 2002). Furthermore, however, it could be also the quality of subdaily precipitation distribution in the  
 573 ERA5 data for the study region, is questionable since on daily, monthly and annual scales ERA5 did not show a significant  
 574 difference with the station data, which could account for that high differences in daily and hourly performance.

### 575 54.3. Reliability of eddy-covariance measurements

576 Reliability of the evaporation measurements using with eddy-covariance technique themselves is a widely discussed question.  
 577 Standard methods of the “energy-balance-closure” corrections (Wilson et al., 2002; Richardson et al., 2012) does not always  
 578 lead to necessary BIAS adjustment (Foken, 2008; Imukova et al., 2016). Therefore, largest systematic deviations between  
 579 observed and modelled evaporation, which could be discussed in the context of inaccuracy of the measurements, were

580 discovered in the evergreen forests in winter, in grassland in summer and in pasture in growing season. Analysis of the  
581 evaporation components and comparison of the FAO with the BROOK90 grass-reference evaporation helped to reveal  
582 some discrepancies in the eddy-covariance measurements.

583 ~~FAO simulations of field sites (Grillenburg and Klingenberg) fit with the observed data quite well, while BROOK90 showed~~  
584 ~~time lag and underestimation of evaporation in summer months.~~ The time lag during the growing and harvesting periods for  
585 Klingenberg could be explained with permanent crop rotation and inability of FAO and BROOK90 models to cope with non-  
586 stationarity in vegetation parameters. Overestimation in winter for the FAO method for both sites could be a result of  
587 simplifications of FAO-modified PM equation against SW approach in BROOK90 (i.e. neglecting the soil water holding  
588 capacity). According to the continuous long-term measurements of grass height in Grillenburg, regular grass cutting is  
589 performed in June-July. This in general should lead to evaporation decline, which can be seen clearly on Fig. 4 for monthly  
590 evaporation of BR90. However, this effect was not found in the measurements (even on a daily scale). Moreover, mean  
591 evaporation usually shows maximum annual values in July. Besides possible systematic measurement errors, this could be  
592 explained either by an underestimation of the real site footprint ~~or by permanent~~. Another explanation is near-saturation  
593 conditions of the soils. Thus, almost unlimited water supply and perturbation of the evaporation components after grass cutting  
594 (drastic increase of soil evaporation). Nevertheless, while calibrating the model, it was realized that it is impossible to increase  
595 soil evaporation by almost 30 mm during the summer months and stay within the physically meaningful boundaries for soil  
596 parameters for the given soil profile. The findings are consistent with other studies, where latent heat fluxes  
597 were systematically over- and underestimated depending on season in in short canopies (Moorhead et al., 2019; Perez-Priego  
598 et al., 2017; Twine et al., 2000).

599 In Tharandt and Oberbaerenburg ~~FAO evaporations are higher than the measurements, especially in summer months, while~~  
600 ~~BROOK90 gave similar values for Tharandt and lower for Oberbaerenburg. In winter months,~~ FAO approach showed 10-20  
601 mm evaporation in the winter months, while BROOK90 resulted in 3-5 mm (consisting only of soil and snow evaporation).  
602 At the same time, all model setups showed 20-30 mm of evaporation per month in winter (which is more than 80 % consists  
603 of intercepted precipitation), while only 5-10 mm is observed. Thus, it is possible that the interception is generally  
604 underestimated by eddy-covariance measurements in the forests. Moreover, while the calibration in Tharandt helped to adjust  
605 the simulated evaporation in winter months as well (primarily by increasing the winter albedo), in Oberbaerenburg even a  
606 relatively wide parameters' range was not sufficient. Here, the large variations between two approaches emphasize the  
607 importance of the soil and in a regulation of the evaporation, since different soil types appear at the grassland and evergreen  
608 forest sites (gleysols and podzols respectively). As few researchers pointed out, that the reliability of eddy-covariance data  
609 within the rainy days and when the interception dominates is indeed questionable (Dijk et al., 2015; Wilson et al., 2001).

610 In addition, previous analysis of eddy-covariance data for some of the study sites showed, that the possible under and  
611 overestimations in measurements could be as large as  $\pm 8-11$  % for Tharandt,  $\pm 29-36$  % for Grillenburg and  $\pm 28-44$  % for  
612 Klingenberg (Spank et al., 2013).

613 Therefore, in addition to reliability of the mean net energy and precipitation (Sect. ~~5.1 and 5.22.4 and 4.2~~), it is possible that  
614 the quality of the eddy-covariance data is questionable due to at least systematic underestimation of interception and non-  
615 representative footprint.

## 616 **Conclusion and outlook**

617 This study presents the qualitative analysis and discussion of the BROOK90 model ~~scale~~ uncertainties with regard to  
618 evaporation simulations. We tried to answer the question ~~how the model setup scale influence~~ influences the performance and  
619 whether the model is more sensitive to the parameter set or to the meteorological input. ~~We For this, used~~ three frameworks  
620 (Global BROOK90, EXTRUSO and BROOK90 with manual parameterization) and three forcing datasets (ERA5, RaKliDa,  
621 in-situ measurements) were used, representing the global, regional and local scale, respectively. We made cross-combinations  
622 of them and model evaporation components for five locations in Saxony, Germany, covered by long-term eddy-covariance  
623 measurements: grassland (Grillenburg), cropland (Klingenberg), deciduous broadleaf forest (Hetzdorf) and two evergreen  
624 needleleaf forests (Tharandt, Oberbaerenburg).

625 Our results indicated that all setups perform well even on a daily scale, with KGE values ranging from 0.35-0.80. KGE  
626 decomposition demonstrated that with high correlation coefficients in grassland, cropland and deciduous forest performance  
627 was affected here mainly by BIAS and variance ratios, whereas in evergreen forest all three components varied greatly. The  
628 highest and lowest values among all setups were achieved by the same combination of Global BROOK90 and ERA5 in  
629 Hetzdorf and Grillenburg respectively. Calibration of the model helped to increase KGE significantly, especially for  
630 Grillenburg and Tharandt. ~~In The~~ vegetation period ~~where when~~ 90-95 % of the total annual evaporation ~~is was~~ observed,  
631 showed the agreement with the observations is was much higher ~~agreement with the observations~~ than in the winter period.

632 The main finding of the study is ~~that for all tested setups, that the spread in model performances is four times higher due to the~~  
633 parameterisation datasets gave us approximately four times higher spread in model performance than compared to the  
634 meteorological forcings based on the tested setups for fields and evergreen forests sites. The opposite was observed in young  
635 deciduous forest for all sites. While Furthermore, while the spread of model performances difference in due to parameter sets  
636 mattered throughout the year, the ~~difference spread due into~~ the meteorological datasets was evident only in summer months.  
637 ~~Analysis of the~~ The breakdown of evaporation components revealed that in the vegetation period transpiration yields up to 65-  
638 75 % of total evaporation, while in the winter ~~months months~~ interception (in forests) and soil/snow evaporation (in fields)  
639 play a major role. Moreover, different the studied parameter sets showed substantial differences in the redistribution of

640 evaporation components. Finally, the [discussion results](#) raised ~~the~~ questions ~~of about~~ meteorological data quality, limitations  
641 of the model and [the](#) reliability of the eddy-covariance measurements ~~as model~~ [evaporation benchmark data](#). [Finally our results](#)  
642 [suggested that the ERA5 dataset works as a meteorological forcing of choice even for a local scale.](#)

643 In the outlook, we would like to suggest possible future directions on this topic:

- 644 • expand the number of study sites with other FLUXNET towers
- 645 • run similar analysis for other physically-based models
- 646 • analyse model uncertainty by incorporating runoff and soil moisture in the analysis
- 647 • apply and validate different methods to breakdown eddy-covariance data in components

648 **Appendix A. Comparison of BROOK90 meteorological input data (ERA5, RaKliDa and station measurements)**

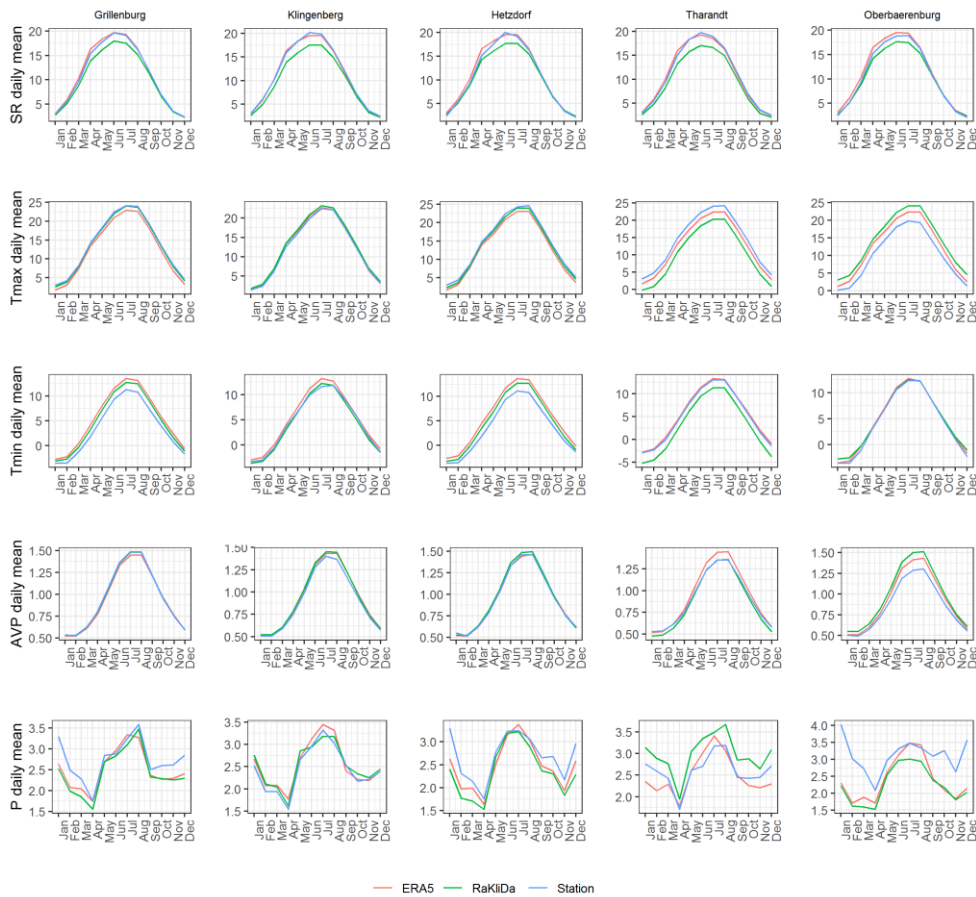


**Figure A1 Monthly daily mean meteorological variables**

Отформатировано: английский (Соединенное Королевство)

649  
650

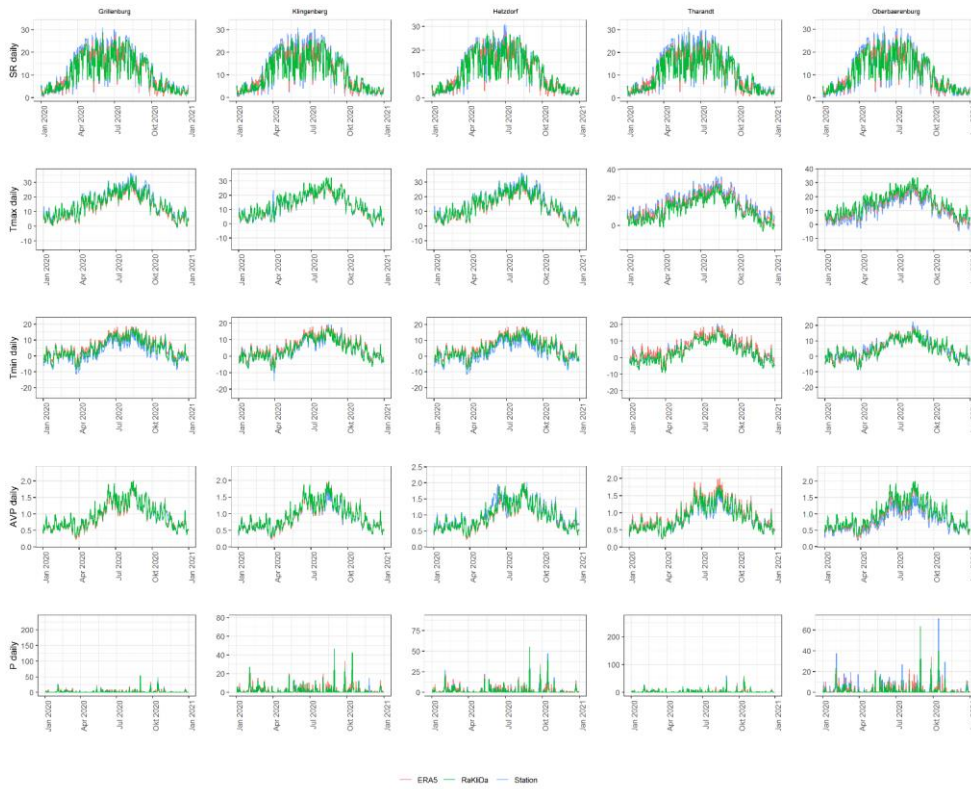


Figure A2 Daily values of meteorological variables for 2020

651  
652  
653























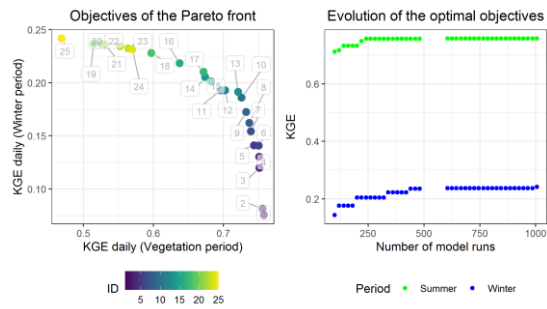






674

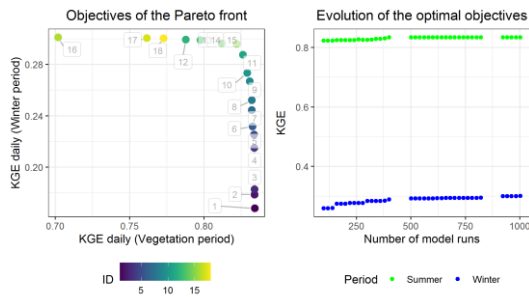
Figure C1 Resulted calibration Pareto fronts for Grillenburg (chosen ID – 9)



675

676

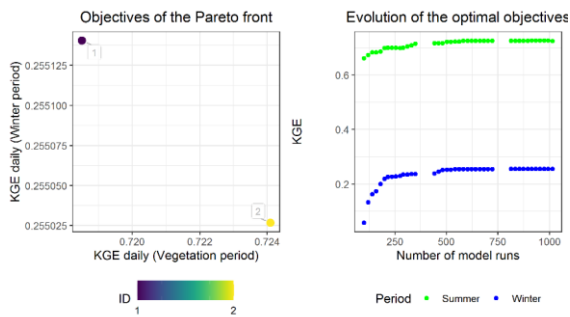
Figure C2 Resulted calibration Pareto fronts for Klingenberg (chosen ID – 13)



677

678

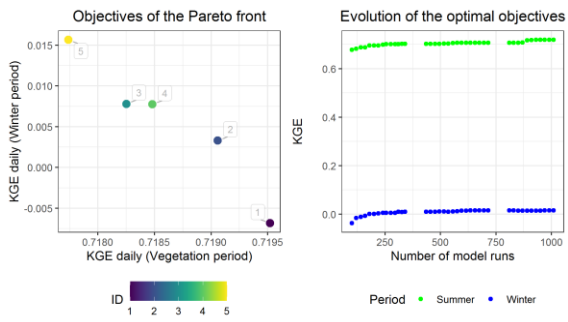
Figure C3 Resulted calibration Pareto fronts for Hetzdorf (chosen ID – 15)



679

680

Figure C4 Resulted calibration Pareto fronts for Tharandt (chosen ID – 2)



681

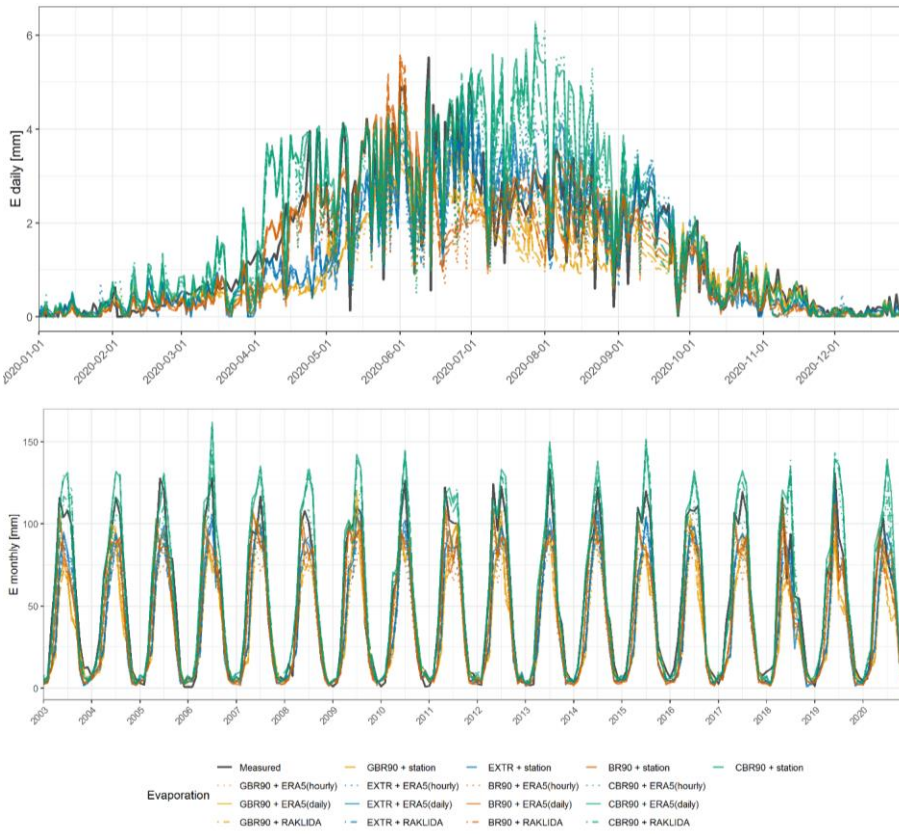
682

Figure C5 Resulted calibration Pareto fronts for Oberbaerenburg (chosen ID – 5)

683

684 **Appendix D. Daily (2020) and monthly (whole time-series) simulations**

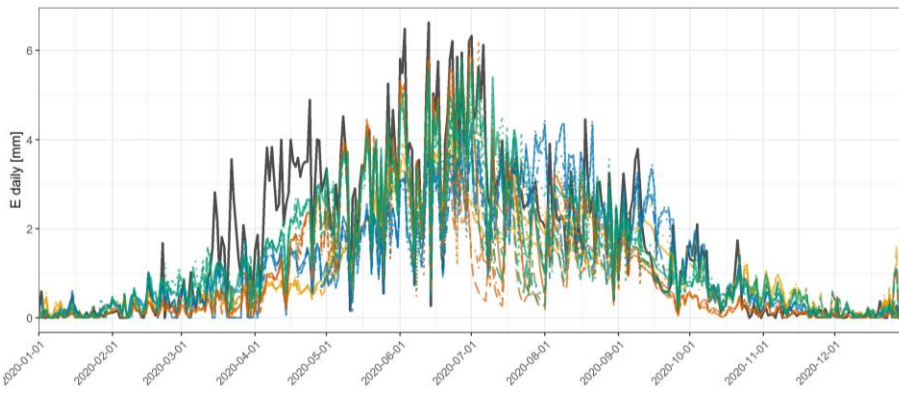
685



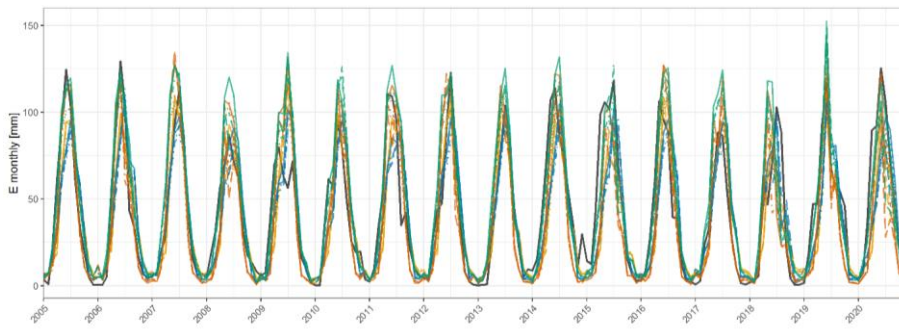
686

687

**Figure D1 Grillenburg**



688

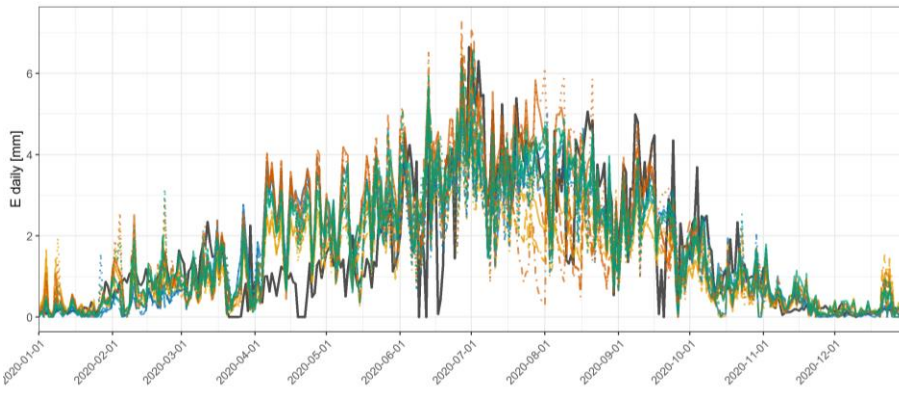


— Measured    — GBR90 + station    — EXTR + station    — BR90 + station    — CBR90 + station  
 - - - GBR90 + ERA5(hourly)    - - - EXTR + ERA5(hourly)    - - - BR90 + ERA5(hourly)    - - - CBR90 + ERA5(hourly)  
 — GBR90 + ERA5(daily)    — EXTR + ERA5(daily)    — BR90 + ERA5(daily)    — CBR90 + ERA5(daily)  
 - - - GBR90 + RAKLIDA    - - - EXTR + RAKLIDA    - - - BR90 + RAKLIDA    - - - CBR90 + RAKLIDA

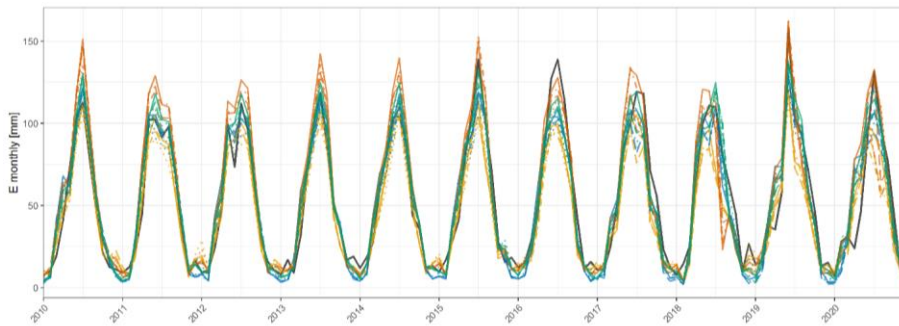
689

690

Figure D2 Klingenberg



691

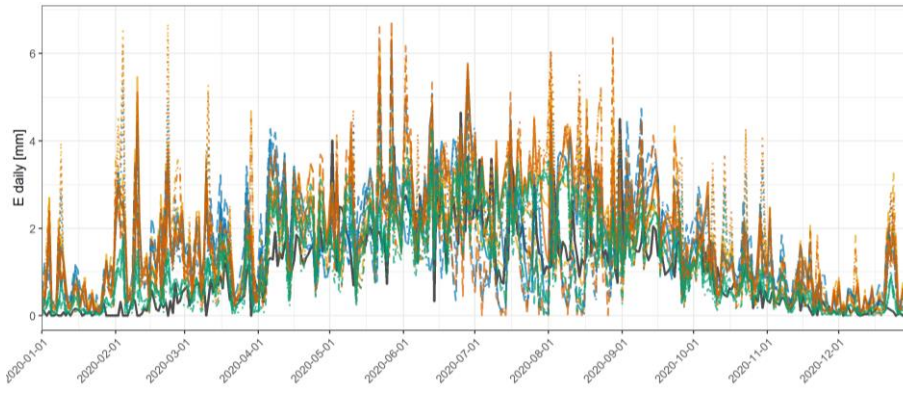


692

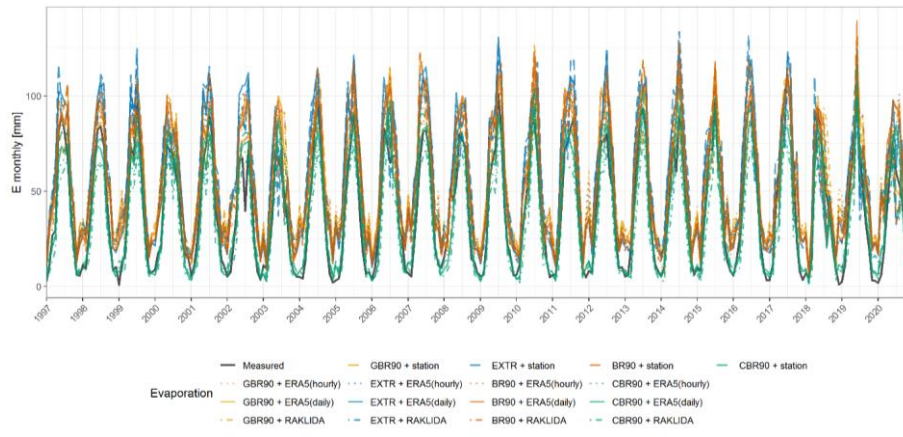
693

**Figure D3 Hetzdorf**

694



695



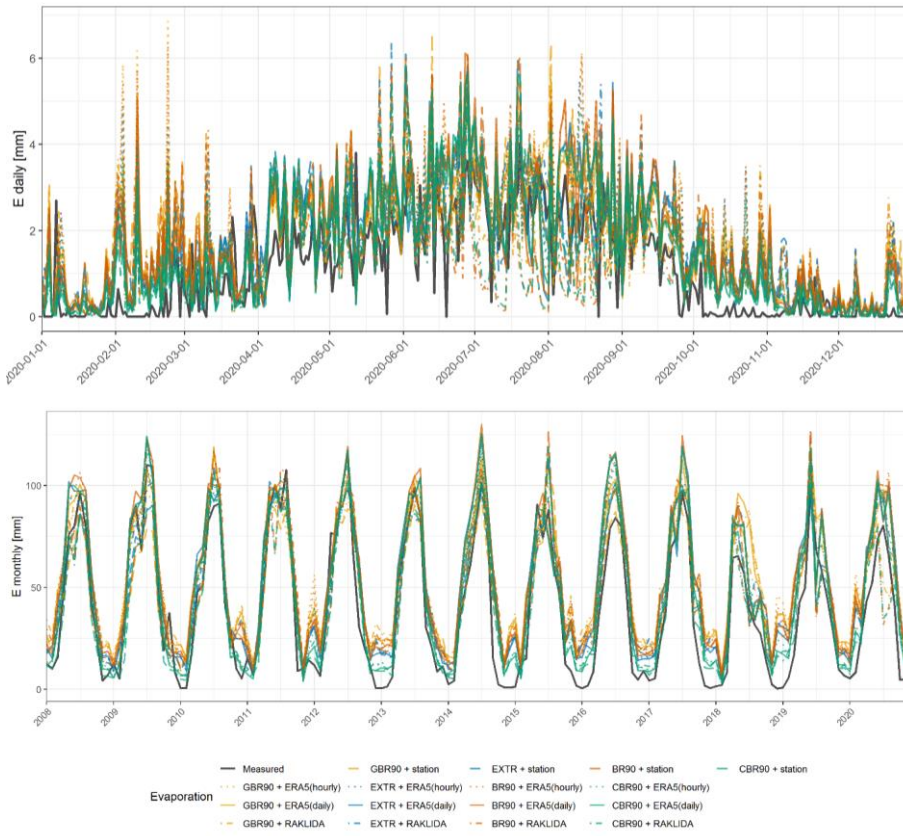
696

Figure D4 Tharandt

— Measured      — GBR90 + station      — EXTR + station      — BR90 + station      — CBR90 + station  
 - - - GBR90 + ERA5(hourly)      - - - EXTR + ERA5(hourly)      - - - BR90 + ERA5(hourly)      - - - CBR90 + ERA5(hourly)  
 — GBR90 + ERA5(daily)      — EXTR + ERA5(daily)      — BR90 + ERA5(daily)      — CBR90 + ERA5(daily)  
 - - - GBR90 + RAKLIDA      - - - EXTR + RAKLIDA      - - - BR90 + RAKLIDA      - - - CBR90 + RAKLIDA



697



698

699

700

Figure D5 Oberbaerenburg







BR90	Station	0.56	0.62	0.58	0.89	0.76
	ERA5 h	0.64	0.65	0.7	0.85	0.94
	ERA5 d	0.59	0.67	0.65	0.74	0.86
	RaKliDa	0.59	0.66	0.67	0.85	0.92
CBR90	Station	0.55	0.67	0.61	0.85	0.82
	ERA5 h	0.52	0.66	0.64	0.5	0.73
	ERA5 d	0.48	0.64	0.57	0.47	0.69
	RaKliDa	0.46	0.62	0.58	0.6	0.73
	Station	0.42	0.61	0.54	0.5	0.63

Отформатировано: английский (Соединенное Королевство)

Отформатировано: английский (Соединенное Королевство)

Отформатировано: английский (Соединенное Королевство)

Отформатировано: английский (Соединенное Королевство)

Отформатировано: английский (Соединенное Королевство)

Отформатировано: английский (Соединенное Королевство)

Отформатировано: английский (Соединенное Королевство)

Отформатировано: английский (Соединенное Королевство)

Отформатировано: английский (Соединенное Королевство)

Отформатировано: английский (Соединенное Королевство)

Отформатировано: английский (Соединенное Королевство)

Отформатировано: английский (Соединенное Королевство)

Отформатировано: английский (Соединенное Королевство)

Отформатировано: английский (Соединенное Королевство)

Отформатировано: английский (Соединенное Королевство)

Отформатировано: английский (Соединенное Королевство)

Отформатировано: английский (Соединенное Королевство)

Отформатировано: английский (Соединенное Королевство)

Отформатировано: английский (Соединенное Королевство)

Отформатировано: английский (Соединенное Королевство)

Отформатировано: английский (Соединенное Королевство)

Отформатировано: английский (Соединенное Королевство)

Отформатировано: английский (Соединенное Королевство)

Отформатировано: английский (Соединенное Королевство)

Отформатировано

Table E2. Daily evaporation skill-scores for the vegetation period

Model/Station	Grillenburg	Klingenberg	Hetzdorf	Tharandt	Oberbaerenburg	
NSE						
GBR90	ERA5 h	-0.46	-0.13	0.09	-0.12	-0.33
	ERA5 d	-0.52	-0.07	0.33	0.06	-0.09
	RaKliDa	-0.64	-0.13	0.28	0	-0.06
	Station	-0.45	-0.08	0.33	0.08	0.04
EXTR	ERA5 h	0.17	-0.08	0.21	0.03	-0.07
	ERA5 d	0.33	0.08	0.4	0.14	0.1
	RaKliDa	0.26	-0.09	0.4	0.15	0.14
	Station	0.41	0.09	0.47	0.12	0.27
BR90	ERA5 h	0.19	0.38	0.43	-0.03	-0.11
	ERA5 d	0.39	0.41	0.53	0.2	0.13
	RaKliDa	0.35	0.37	0.52	0.08	0.08
	Station	0.43	0.37	0.58	0.2	0.26
CBR90	ERA5 h	0.62	0.24	0.3	0.22	0.11
	ERA5 d	0.72	0.37	0.52	0.37	0.32
	RaKliDa	0.75	0.38	0.51	0	0.23
	Station	0.78	0.42	0.59	0.45	0.42
KGE						
GBR90	ERA5 h	0.33	0.49	0.57	0.38	0.39
	ERA5 d	0.34	0.52	0.67	0.54	0.53
	RaKliDa	0.28	0.48	0.64	0.39	0.49
	Station	0.33	0.51	0.66	0.47	0.54
EXTR	ERA5 h	0.51	0.5	0.63	0.48	0.52
	ERA5 d	0.59	0.57	0.71	0.55	0.59
	RaKliDa	0.53	0.49	0.71	0.49	0.58
	Station	0.6	0.56	0.74	0.46	0.64
BR90	ERA5 h	0.53	0.66	0.68	0.39	0.45
	ERA5 d	0.67	0.68	0.71	0.56	0.58
	RaKliDa	0.64	0.66	0.7	0.41	0.51
	Station	0.66	0.65	0.75	0.46	0.61
CBR90	ERA5 h	0.81	0.65	0.67	0.63	0.58
	ERA5 d	0.82	0.68	0.77	0.7	0.67
	RaKliDa	0.84	0.7	0.76	0.51	0.62
	Station	0.87	0.71	0.8	0.71	0.71
Correlation						
GBR90	ERA5 h	0.67	0.61	0.68	0.43	0.43

	ERA5 d	0.66	0.63	0.75	0.59	0.6
	RaKliDa	0.67	0.64	0.73	0.42	0.52
	Station	0.71	0.64	0.76	0.58	0.55
EXTR	ERA5 h	0.81	0.66	0.67	0.55	0.56
	ERA5 d	0.83	0.68	0.74	0.64	0.65
	RaKliDa	0.83	0.66	0.73	0.57	0.6
	Station	0.85	0.69	0.76	0.57	0.65
BR90	ERA5 h	0.79	0.7	0.7	0.45	0.49
	ERA5 d	0.78	0.69	0.76	0.62	0.64
	RaKliDa	0.8	0.69	0.74	0.45	0.54
	Station	0.82	0.68	0.78	0.59	0.62
CBR90	ERA5 h	0.81	0.66	0.69	0.67	0.61
	ERA5 d	0.87	0.72	0.78	0.72	0.71
	RaKliDa	0.88	0.72	0.77	0.61	0.64
	Station	0.89	0.72	0.8	0.72	0.71
BIAS						
GBR90	ERA5 h	0.68	0.83	0.83	1.22	1.22
	ERA5 d	0.72	0.9	0.88	1.26	1.27
	RaKliDa	0.68	0.85	0.84	1.07	1.2
	Station	0.69	0.85	0.84	1.34	1.1
EXTR	ERA5 h	0.73	0.88	0.97	1.29	1.22
	ERA5 d	0.77	0.94	1.03	1.32	1.26
	RaKliDa	0.73	0.87	0.99	1.23	1.15
	Station	0.76	0.9	1	1.32	1.11
BR90	ERA5 h	0.74	0.87	1.04	1.23	1.25
	ERA5 d	0.84	0.96	1.12	1.24	1.27
	RaKliDa	0.81	0.88	1.07	1.05	1.18
	Station	0.81	0.88	1.05	1.29	1.1
CBR90	ERA5 h	0.99	1.06	0.99	0.89	1.15
	ERA5 d	1.13	1.17	1.05	0.94	1.2
	RaKliDa	1.11	1.08	1	0.78	1.11
	Station	1.07	1.08	1	1.01	1.03
Variance ratio						
GBR90	ERA5 h	0.55	0.62	0.71	1.32	0.87
	ERA5 d	0.5	0.6	0.72	1.13	0.77
	RaKliDa	0.49	0.57	0.8	1.45	0.97
	Station	0.51	0.6	0.75	1.59	0.91
EXTR	ERA5 h	0.63	0.56	0.75	1.33	0.83
	ERA5 d	0.67	0.61	0.78	1.31	0.85
	RaKliDa	0.65	0.55	0.85	1.48	0.97
	Station	0.7	0.61	0.83	1.68	0.97
BR90	ERA5 h	0.67	1.05	1.2	1.49	1.03
	ERA5 d	0.75	1.15	1.29	1.3	0.99
	RaKliDa	0.72	1.07	1.36	1.59	1.14
	Station	0.72	1.11	1.22	1.84	1.1
CBR90	ERA5 h	0.99	0.83	0.81	0.81	0.86
	ERA5 d	1.1	0.96	0.91	0.85	0.92
	RaKliDa	1.1	0.89	0.93	0.86	0.95
	Station	1.07	0.96	0.96	1.06	1.02

Отформатировано: английский (Соединенное Королевство)

Отформатировано: английский (Соединенное Королевство)

Отформатировано: английский (Соединенное Королевство)

Отформатировано: английский (Соединенное Королевство)

Отформатировано: английский (Соединенное Королевство)

Отформатировано: английский (Соединенное Королевство)

Отформатировано: английский (Соединенное Королевство)

Отформатировано: английский (Соединенное Королевство)

Отформатировано: английский (Соединенное Королевство)

Отформатировано: английский (Соединенное Королевство)

Отформатировано: английский (Соединенное Королевство)

Отформатировано: английский (Соединенное Королевство)

Отформатировано: английский (Соединенное Королевство)

		MAE				
GBR90	ERA5 h	1.04	0.91	0.87	0.92	1.05
	ERA5 d	0.98	0.87	0.74	0.83	0.95
	RaKliDa	1.02	0.86	0.83	0.95	0.98
	Station	0.95	0.86	0.76	0.93	0.95
EXTR	ERA5 h	0.86	0.86	0.83	0.91	0.95
	ERA5 d	0.79	0.83	0.73	0.88	0.94
	RaKliDa	0.83	0.85	0.77	0.89	0.9
BR90	Station	0.74	0.82	0.7	1.02	0.85
	ERA5 h	0.85	0.87	0.88	0.93	1.05
	ERA5 d	0.77	0.89	0.82	0.81	0.97
	RaKliDa	0.77	0.88	0.84	0.94	1.03
CBR90	Station	0.72	0.89	0.75	0.94	0.91
	ERA5 h	0.68	0.88	0.8	0.63	0.87
	ERA5 d	0.63	0.85	0.7	0.58	0.83
	RaKliDa	0.59	0.81	0.72	0.76	0.87
Station	0.53	0.8	0.65	0.61	0.77	

Отформатировано: английский (Соединенное Королевство)

Отформатировано: английский (Соединенное Королевство)

Отформатировано: английский (Соединенное Королевство)

Отформатировано: английский (Соединенное Королевство)

Отформатировано: английский (Соединенное Королевство)

Table E3. Daily evaporation skill-scores for the winter period

Model/Station	Grillenbug	Klingenberg	Hetzdorf	Tharandt	Oberbaerenburg	
NSE						
GBR90	ERA5 h	-0.86	-2.08	-0.3	-0.42	-0.79
	ERA5 d	-0.7	-1.8	-0.47	-0.56	-1.13
	RaKliDa	-0.56	-1.54	-0.51	-0.36	-0.91
	Station	-0.54	-1.22	-0.5	-0.57	-0.6
EXTR	ERA5 h	-1.05	-2.42	-0.85	-0.44	-0.96
	ERA5 d	-1.13	-2.14	-1.33	-0.52	-1.3
	RaKliDa	-0.98	-1.69	-1.58	-0.42	-0.9
BR90	Station	-1.19	-1.29	-1.6	-0.56	-0.82
	ERA5 h	-2.07	-4.25	-0.29	-0.37	-0.8
	ERA5 d	-1.81	-3.67	-0.37	-0.46	-1.2
	RaKliDa	-1.48	-2.94	-0.41	-0.32	-0.94
CBR90	Station	-1.83	-2.13	-0.43	-0.46	-0.67
	ERA5 h	-0.26	-1.5	-0.16	-0.61	-1.16
	ERA5 d	-0.21	-1.4	-0.41	-0.66	-1.93
	RaKliDa	-0.08	-1.23	-0.4	-0.83	-1.34
Station	-0.05	-0.96	-0.64	-0.34	-1.6	
KGE						
GBR90	ERA5 h	0.24	-0.04	0.15	-0.32	-0.38
	ERA5 d	0.3	0.02	0.25	-0.21	-0.32
	RaKliDa	0.32	0.06	0.17	-0.29	-0.33
	Station	0.34	0.12	0.13	-0.22	-0.2
EXTR	ERA5 h	0.17	-0.13	0.07	-0.22	-0.27
	ERA5 d	0.11	-0.06	-0.1	-0.1	-0.22
	RaKliDa	0.14	0.06	-0.18	-0.14	-0.26
BR90	Station	0.05	0.14	-0.22	-0.14	-0.15
	ERA5 h	-0.22	-0.63	0.22	-0.3	-0.35
	ERA5 d	-0.17	-0.52	0.3	-0.16	-0.28

Отформатировано: английский (Соединенное Королевство)

Отформатировано: английский (Соединенное Королевство)

Отформатировано: английский (Соединенное Королевство)

Отформатировано: английский (Соединенное Королевство)

Отформатировано: английский (Соединенное Королевство)

Отформатировано: английский (Соединенное Королевство)

Отформатировано: английский (Соединенное Королевство)

Отформатировано: английский (Соединенное Королевство)

Отформатировано: английский (Соединенное Королевство)

Отформатировано: английский (Соединенное Королевство)

	RaKliDa	-0.06	-0.32	0.24	-0.26	-0.28
	Station	-0.2	-0.16	0.19	-0.19	-0.17
GBR90	ERA5 h	0.41	0.1	0.32	0.22	-0.16
	ERA5 d	0.43	0.12	0.33	0.26	-0.15
	RaKliDa	0.45	0.15	0.3	0.12	-0.11
	Station	0.49	0.2	0.22	0.26	-0.02
Correlation						
GBR90	ERA5 h	0.33	0.21	0.19	0.14	-0.06
	ERA5 d	0.36	0.24	0.25	0.21	-0.05
	RaKliDa	0.35	0.2	0.19	0.15	-0.02
	Station	0.42	0.22	0.15	0.24	0.13
EXTR	ERA5 h	0.32	0.29	0.28	0.18	-0.04
	ERA5 d	0.27	0.24	0.34	0.27	-0.03
	RaKliDa	0.25	0.25	0.28	0.26	-0.02
	Station	0.32	0.24	0.28	0.29	0.08
BR90	ERA5 h	0.2	0.05	0.24	0.13	-0.07
	ERA5 d	0.19	0.05	0.31	0.21	-0.05
	RaKliDa	0.22	0.03	0.25	0.14	-0.01
	Station	0.29	0.06	0.21	0.23	0.1
GBR90	ERA5 h	0.42	0.26	0.34	0.22	-0.05
	ERA5 d	0.44	0.29	0.37	0.28	-0.03
	RaKliDa	0.46	0.26	0.34	0.15	0.02
	Station	0.5	0.27	0.3	0.28	0.11
BIAS						
GBR90	ERA5 h	0.85	1.15	1.01	3.45	3.92
	ERA5 d	0.9	1.23	0.92	3.15	3.69
	RaKliDa	0.94	1.29	0.88	3.13	3.97
	Station	0.83	1.3	0.9	3.46	3.59
EXTR	ERA5 h	0.76	0.85	0.63	2.91	2.97
	ERA5 d	0.71	0.83	0.55	2.72	2.83
	RaKliDa	0.74	0.95	0.53	2.79	3.11
	Station	0.65	0.98	0.51	3.1	2.91
BR90	ERA5 h	0.57	0.56	0.97	3.15	3.49
	ERA5 d	0.59	0.57	0.9	2.75	3.16
	RaKliDa	0.62	0.64	0.88	2.76	3.46
	Station	0.56	0.69	0.9	3.01	3.11
GBR90	ERA5 h	1.05	1.12	0.96	1.01	2
	ERA5 d	1	1.11	0.81	0.98	1.78
	RaKliDa	1.1	1.2	0.8	0.82	2.01
	Station	0.96	1.24	0.75	1.21	1.62
Variance ratio						
GBR90	ERA5 h	0.59	0.36	1.7	11.57	3.47
	ERA5 d	0.63	0.4	1.05	6.56	2.15
	RaKliDa	0.73	0.49	1.19	10.35	2.86
	Station	0.65	0.57	1.35	7.88	2.87
EXTR	ERA5 h	0.54	0.29	0.85	6.8	1.88
	ERA5 d	0.57	0.34	0.61	4.38	1.26
	RaKliDa	0.65	0.41	0.6	5.53	2.02
	Station	0.52	0.51	0.61	5.61	1.74

Отформатировано: английский (Соединенное Королевство)

Отформатировано: английский (Соединенное Королевство)

Отформатировано: английский (Соединенное Королевство)

Отформатировано: английский (Соединенное Королевство)

Отформатировано: английский (Соединенное Королевство)

Отформатировано: английский (Соединенное Королевство)

Отформатировано: английский (Соединенное Королевство)

Отформатировано: английский (Соединенное Королевство)

Отформатировано: английский (Соединенное Королевство)

Отформатировано: английский (Соединенное Королевство)

Отформатировано: английский (Соединенное Королевство)

Отформатировано: английский (Соединенное Королевство)

Отформатировано: английский (Соединенное Королевство)

Отформатировано: английский (Соединенное Королевство)

BR90	ERA5 h	0.42	0.24	1.43	10.51	2.91
	ERA5 d	0.47	0.27	1.03	5.42	1.64
	RaKliDa	0.53	0.34	1.17	8.52	2.23
	Station	0.42	0.45	1.27	6.6	2.21
CBR90	ERA5 h	0.86	0.44	1.37	0.93	1.1
	ERA5 d	0.86	0.44	0.88	0.78	0.6
	RaKliDa	1.02	0.52	0.98	0.89	0.86
	Station	0.92	0.62	0.86	1.22	0.56
MAE						
GBR90	ERA5 h	0.19	0.23	0.36	0.75	0.8
	ERA5 d	0.19	0.23	0.32	0.67	0.74
	RaKliDa	0.19	0.24	0.34	0.73	0.78
	Station	0.18	0.24	0.36	0.74	0.69
EXTR	ERA5 h	0.19	0.19	0.31	0.61	0.61
	ERA5 d	0.2	0.2	0.31	0.55	0.58
	RaKliDa	0.2	0.2	0.32	0.57	0.64
	Station	0.19	0.21	0.32	0.65	0.57
BR90	ERA5 h	0.21	0.21	0.33	0.69	0.72
	ERA5 d	0.21	0.22	0.3	0.58	0.65
	RaKliDa	0.21	0.22	0.33	0.66	0.69
	Station	0.2	0.23	0.34	0.64	0.62
CBR90	ERA5 h	0.2	0.22	0.31	0.25	0.45
	ERA5 d	0.19	0.21	0.28	0.24	0.41
	RaKliDa	0.19	0.22	0.29	0.26	0.44
	Station	0.18	0.23	0.3	0.27	0.36

Отформатировано: английский (Соединенное Королевство)

Отформатировано: английский (Соединенное Королевство)

Отформатировано: английский (Соединенное Королевство)

Отформатировано: английский (Соединенное Королевство)

Отформатировано: английский (Соединенное Королевство)

Отформатировано: английский (Соединенное Королевство)

Отформатировано: английский (Соединенное Королевство)

Table E4. Monthly evaporation skill-scores for the whole year

Model/Station	Grillenbug	Klingenberg	Hetzdorf	Tharandt	Oberbaerenburg	
NSE						
GBR90	ERA5 h	0.37	0.56	0.74	0.44	0.49
	ERA5 d	0.49	0.65	0.84	0.57	0.59
	RaKliDa	0.37	0.59	0.78	0.54	0.54
	Station	0.4	0.56	0.77	0.47	0.55
EXTR	ERA5 h	0.63	0.61	0.84	0.59	0.7
	ERA5 d	0.74	0.68	0.88	0.61	0.71
	RaKliDa	0.66	0.55	0.88	0.63	0.72
	Station	0.72	0.6	0.89	0.48	0.75
BR90	ERA5 h	0.65	0.77	0.89	0.57	0.63
	ERA5 d	0.84	0.77	0.88	0.69	0.69
	RaKliDa	0.8	0.74	0.88	0.67	0.63
	Station	0.81	0.72	0.9	0.6	0.72
CBR90	ERA5 h	0.93	0.83	0.9	0.84	0.84
	ERA5 d	0.92	0.79	0.92	0.9	0.85
	RaKliDa	0.93	0.81	0.92	0.67	0.83
	Station	0.93	0.79	0.93	0.91	0.87
KGE						
GBR90	ERA5 h	0.41	0.68	0.66	0.67	0.65
	ERA5 d	0.51	0.79	0.79	0.71	0.69

	RaKliDa	0.43	0.72	0.71	0.69	0.66
	Station	0.44	0.72	0.72	0.67	0.67
EXTR	ERA5 h	0.54	0.71	0.86	0.71	0.74
	ERA5 d	0.65	0.82	0.94	0.69	0.74
	RaKliDa	0.57	0.7	0.91	0.73	0.75
	Station	0.62	0.75	0.92	0.67	0.77
BR90	ERA5 h	0.54	0.8	0.94	0.72	0.71
	ERA5 d	0.76	0.82	0.84	0.74	0.72
	RaKliDa	0.7	0.8	0.89	0.76	0.72
	Station	0.7	0.8	0.91	0.7	0.77
CBR90	ERA5 h	0.96	0.9	0.89	0.82	0.83
	ERA5 d	0.82	0.79	0.94	0.91	0.8
	RaKliDa	0.85	0.86	0.95	0.65	0.84
	Station	0.88	0.85	0.96	0.95	0.91
Correlation						
GBR90	ERA5 h	0.92	0.86	0.96	0.91	0.91
	ERA5 d	0.91	0.86	0.95	0.94	0.94
	RaKliDa	0.91	0.85	0.96	0.89	0.93
	Station	0.91	0.84	0.95	0.94	0.89
EXTR	ERA5 h	0.95	0.87	0.94	0.93	0.94
	ERA5 d	0.95	0.86	0.94	0.93	0.94
	RaKliDa	0.95	0.85	0.95	0.92	0.94
	Station	0.95	0.85	0.95	0.89	0.93
BR90	ERA5 h	0.96	0.9	0.95	0.92	0.93
	ERA5 d	0.96	0.88	0.95	0.94	0.94
	RaKliDa	0.96	0.88	0.94	0.9	0.91
	Station	0.96	0.87	0.95	0.93	0.92
CBR90	ERA5 h	0.97	0.92	0.96	0.95	0.95
	ERA5 d	0.98	0.91	0.96	0.95	0.95
	RaKliDa	0.98	0.91	0.96	0.93	0.94
	Station	0.97	0.9	0.96	0.96	0.94
BIAS						
GBR90	ERA5 h	0.69	0.84	0.85	1.38	1.37
	ERA5 d	0.72	0.91	0.89	1.39	1.4
	RaKliDa	0.7	0.87	0.84	1.22	1.35
	Station	0.7	0.87	0.85	1.49	1.23
EXTR	ERA5 h	0.73	0.88	0.94	1.4	1.31
	ERA5 d	0.77	0.94	0.99	1.42	1.35
	RaKliDa	0.73	0.87	0.95	1.34	1.26
	Station	0.75	0.9	0.95	1.44	1.21
BR90	ERA5 h	0.73	0.86	1.03	1.36	1.37
	ERA5 d	0.83	0.94	1.1	1.34	1.38
	RaKliDa	0.8	0.87	1.05	1.17	1.31
	Station	0.8	0.87	1.04	1.41	1.21
CBR90	ERA5 h	0.99	1.06	0.99	0.9	1.19
	ERA5 d	1.13	1.16	1.03	0.94	1.23
	RaKliDa	1.11	1.09	0.98	0.78	1.16
	Station	1.07	1.09	0.98	1.02	1.06
Variance ratio						



GBR90	ERA5 h	0.53	0.67	0.61	0.75	0.69
	ERA5 d	0.6	0.8	0.74	0.91	0.81
	RaKliDa	0.54	0.71	0.68	0.66	0.68
	Station	0.56	0.73	0.68	1	0.64
EXTR	ERA5 h	0.62	0.68	0.81	1.01	0.84
	ERA5 d	0.73	0.82	1	1.16	0.97
	RaKliDa	0.66	0.68	0.92	0.98	0.78
	Station	0.71	0.72	0.94	1.09	0.76
BR90	ERA5 h	0.61	1.03	1.03	0.88	0.87
	ERA5 d	0.82	1.28	1.3	1.03	0.99
	RaKliDa	0.75	1.1	1.19	0.75	0.8
	Station	0.76	1.1	1.13	1.1	0.8
CBR90	ERA5 h	0.97	1.01	0.83	0.79	0.95
	ERA5 d	1.36	1.32	1.06	0.9	1.12
	RaKliDa	1.28	1.12	0.95	0.7	0.91
	Station	1.23	1.15	1.01	0.98	0.93
MAE						
GBR90	ERA5 h	17.04	13.93	11.7	16.25	16.99
	ERA5 d	15.94	13.78	9.95	16.05	16.91
	RaKliDa	17.17	14.09	11.05	13.05	16.15
	Station	16.9	14.71	11.22	19.56	15.01
EXTR	ERA5 h	15.12	13.21	10.08	16.85	14.43
	ERA5 d	13.59	13.37	9.82	17.6	15.15
	RaKliDa	14.75	14.32	9.69	15.5	13.14
	Station	13.77	13.93	9.32	19.99	12.26
BR90	ERA5 h	14.6	12.81	9.48	15.45	16.49
	ERA5 d	11.31	13.91	11.25	14.38	15.96
	RaKliDa	12.11	14.09	10.67	11.8	15.29
	Station	11.86	14.47	9.8	17.32	13.02
CBR90	ERA5 h	7.08	10.51	8.36	7.7	10.74
	ERA5 d	9.12	12.59	8.39	6.69	11.16
	RaKliDa	8.24	11.56	8.01	10.93	10.51
	Station	7.9	12.11	7.9	6.35	8.85

Table E5. Monthly evaporation skill-scores for the vegetation period

Model/Station	Grillenburg	Klingenberg	Hetzdorf	Tharandt	Oberbaerenburg	
NSE						
GBR90	ERA5 h	-0.18	0.23	0.5	0.32	0.3
	ERA5 d	0.07	0.4	0.69	0.4	0.41
	RaKliDa	-0.14	0.3	0.58	0.57	0.43
	Station	-0.1	0.27	0.56	0.22	0.48
EXTR	ERA5 h	0.3	0.17	0.59	0.3	0.5
	ERA5 d	0.54	0.35	0.71	0.29	0.49
	RaKliDa	0.39	0.11	0.72	0.42	0.65
	Station	0.49	0.21	0.74	0.13	0.68
BR90	ERA5 h	0.29	0.64	0.78	0.45	0.48
	ERA5 d	0.69	0.65	0.75	0.55	0.53
	RaKliDa	0.62	0.62	0.77	0.68	0.51

Отформатировано: английский (Соединенное Королевство)

Отформатировано: английский (Соединенное Королевство)

Отформатировано: английский (Соединенное Королевство)

Отформатировано: английский (Соединенное Королевство)

Отформатировано: английский (Соединенное Королевство)

	Station	0.63	0.59	0.81	0.41	0.68
GBR90	ERA5 h	0.86	0.66	0.75	0.68	0.72
	ERA5 d	0.83	0.61	0.83	0.79	0.71
	RaKliDa	0.86	0.65	0.84	0.39	0.7
	Station	0.86	0.62	0.86	0.83	0.8
KGE						
GBR90	ERA5 h	0.45	0.63	0.62	0.72	0.62
	ERA5 d	0.54	0.71	0.76	0.77	0.7
	RaKliDa	0.47	0.66	0.69	0.78	0.66
	Station	0.48	0.65	0.7	0.73	0.69
EXTR	ERA5 h	0.59	0.58	0.63	0.74	0.72
	ERA5 d	0.68	0.69	0.78	0.72	0.75
	RaKliDa	0.61	0.58	0.74	0.76	0.76
	Station	0.66	0.62	0.77	0.67	0.79
BR90	ERA5 h	0.57	0.76	0.89	0.78	0.74
	ERA5 d	0.78	0.72	0.82	0.78	0.76
	RaKliDa	0.73	0.72	0.85	0.84	0.75
	Station	0.74	0.71	0.89	0.73	0.82
GBR90	ERA5 h	0.93	0.83	0.75	0.81	0.82
	ERA5 d	0.79	0.75	0.9	0.89	0.82
	RaKliDa	0.82	0.8	0.87	0.67	0.83
	Station	0.85	0.78	0.91	0.91	0.9
Correlation						
GBR90	ERA5 h	0.85	0.75	0.92	0.87	0.88
	ERA5 d	0.83	0.74	0.92	0.91	0.91
	RaKliDa	0.83	0.74	0.92	0.84	0.89
	Station	0.83	0.72	0.91	0.9	0.84
EXTR	ERA5 h	0.91	0.75	0.9	0.87	0.91
	ERA5 d	0.91	0.74	0.9	0.87	0.91
	RaKliDa	0.91	0.7	0.91	0.85	0.91
	Station	0.91	0.71	0.91	0.79	0.89
BR90	ERA5 h	0.93	0.83	0.9	0.88	0.9
	ERA5 d	0.92	0.81	0.9	0.91	0.91
	RaKliDa	0.92	0.81	0.89	0.85	0.86
	Station	0.93	0.79	0.91	0.88	0.88
GBR90	ERA5 h	0.93	0.84	0.92	0.89	0.92
	ERA5 d	0.95	0.83	0.93	0.91	0.92
	RaKliDa	0.95	0.83	0.93	0.87	0.89
	Station	0.94	0.81	0.93	0.91	0.91
BIAS						
GBR90	ERA5 h	0.68	0.83	0.83	1.22	1.22
	ERA5 d	0.72	0.9	0.88	1.26	1.27
	RaKliDa	0.68	0.85	0.84	1.07	1.2
	Station	0.69	0.85	0.84	1.34	1.1
EXTR	ERA5 h	0.73	0.88	0.97	1.29	1.22
	ERA5 d	0.77	0.94	1.03	1.32	1.26
	RaKliDa	0.73	0.87	0.99	1.23	1.15
	Station	0.76	0.9	1	1.32	1.11
BR90	ERA5 h	0.74	0.87	1.04	1.23	1.25

Отформатировано: английский (Соединенное Королевство)

Отформатировано: английский (Соединенное Королевство)

Отформатировано: английский (Соединенное Королевство)

Отформатировано: английский (Соединенное Королевство)

Отформатировано: английский (Соединенное Королевство)

Отформатировано: английский (Соединенное Королевство)

Отформатировано: английский (Соединенное Королевство)

Отформатировано: английский (Соединенное Королевство)

Отформатировано: английский (Соединенное Королевство)

Отформатировано: английский (Соединенное Королевство)

Отформатировано: английский (Соединенное Королевство)

Отформатировано: английский (Соединенное Королевство)

Отформатировано: английский (Соединенное Королевство)

Отформатировано: английский (Соединенное Королевство)

Отформатировано: английский (Соединенное Королевство)

	ERA5 d	0.84	0.96	1.12	1.24	1.27
	RaKliDa	0.81	0.88	1.07	1.05	1.18
	Station	0.81	0.88	1.06	1.29	1.1
	ERA5 h	0.99	1.06	0.99	0.89	1.15
C BR90	ERA5 d	1.13	1.17	1.05	0.94	1.2
	RaKliDa	1.11	1.08	1	0.78	1.11
	Station	1.07	1.08	1	1.01	1.03
Variance ratio						
G BR90	ERA5 h	0.64	0.71	0.58	0.73	0.58
	ERA5 d	0.74	0.86	0.72	0.91	0.7
	RaKliDa	0.69	0.79	0.67	0.77	0.61
	Station	0.69	0.82	0.67	1.03	0.64
EXTR	ERA5 h	0.73	0.59	0.55	0.97	0.7
	ERA5 d	0.9	0.75	0.7	1.14	0.82
	RaKliDa	0.82	0.64	0.65	1.01	0.73
B R90	Station	0.87	0.68	0.68	1.15	0.75
	ERA5 h	0.67	1.23	0.95	0.91	0.78
	ERA5 d	0.91	1.55	1.23	1.1	0.91
C BR90	RaKliDa	0.85	1.37	1.15	0.92	0.78
	Station	0.84	1.37	1.07	1.22	0.86
	ERA5 h	0.97	0.93	0.66	0.83	0.84
C BR90	ERA5 d	1.42	1.29	0.9	0.95	1.01
	RaKliDa	1.35	1.11	0.81	0.84	0.84
	Station	1.31	1.17	0.89	1.03	0.96
MAE						
G BR90	ERA5 h	24.02	18.64	15.24	14.33	15.87
	ERA5 d	22.44	18.33	12.84	15.23	16.54
	RaKliDa	24.23	18.65	14.4	10.68	14.7
	Station	23.78	19.65	14.38	19.24	13.97
EXTR	ERA5 h	20.8	18.05	12.28	17.44	14.9
	ERA5 d	18.27	18.12	11.52	19.34	16.42
	RaKliDa	20.12	19.52	11.16	15.93	12.55
B R90	Station	18.67	18.98	10.45	21.39	11.88
	ERA5 h	19.72	17.03	12.24	14.3	16.36
	ERA5 d	14.77	18.62	15	14.32	16.64
C BR90	RaKliDa	15.99	18.86	13.95	10.23	14.91
	Station	15.58	19.57	12.45	17.71	12.43
	ERA5 h	9.07	13.66	10.68	9.82	11.91
C BR90	ERA5 d	12.11	16.86	10.55	8.35	13.09
	RaKliDa	10.8	15.2	9.89	14.54	11.77
	Station	10.35	16.02	9.58	7.76	10.19

Отформатировано: английский (Соединенное Королевство)

Отформатировано: английский (Соединенное Королевство)

Отформатировано: английский (Соединенное Королевство)

Отформатировано: английский (Соединенное Королевство)

Отформатировано: английский (Соединенное Королевство)

Отформатировано: английский (Соединенное Королевство)

Отформатировано: английский (Соединенное Королевство)

Отформатировано: английский (Соединенное Королевство)

Отформатировано: английский (Соединенное Королевство)

Отформатировано: английский (Соединенное Королевство)

Отформатировано: английский (Соединенное Королевство)

Table E6. Monthly evaporation skill-scores for the winter period

Model/Station	Grillenburg	Klingenberg	Hetzdorf	Tharandt	Oberbaerenburg	
NSE						
G BR90	ERA5 h	-0.84	-3.36	-0.21	-3.65	-3.23
	ERA5 d	-0.62	-2.97	-0.56	-4.55	-4.59
	RaKliDa	-0.48	-2.77	-0.88	-3.28	-4.82

Отформатировано: английский (Соединенное Королевство)

Отформатировано: английский (Соединенное Королевство)

Отформатировано: английский (Соединенное Королевство)

	Station	-0.46	-2.6	-1.21	-6.21	-4.03
EXTR	ERA5 h	-4.44	-5.59	-2.96	-3.47	-3.15
	ERA5 d	-4.71	-6.57	-4.39	-3.68	-3.9
	RaKliDa	-3.93	-5.71	-4.81	-3.62	-3.5
	Station	-4.19	-4.8	-4.49	-5.1	-3.8
BR90	ERA5 h	-8.08	-16.29	-0.02	-3.13	-3
	ERA5 d	-7.88	-14.62	-0.18	-3.66	-4.2
	RaKliDa	-6.26	-9.67	-0.45	-2.75	-4.27
	Station	-6.69	-7.49	-0.91	-4.85	-3.74
CBR90	ERA5 h	-0.4	-1.97	0.27	-0.86	-1.95
	ERA5 d	-0.49	-2.02	-0.21	-0.83	-2.61
	RaKliDa	-0.35	-2.27	-0.23	-2.12	-2.36
	Station	-0.22	-2.08	-0.96	-0.45	-2.65
KGE						
GBR90	ERA5 h	0.27	-0.3	0.32	-0.32	-0.32
	ERA5 d	0.33	-0.21	0.35	-0.22	-0.28
	RaKliDa	0.39	-0.15	0.27	-0.34	-0.2
	Station	0.4	-0.11	0.09	-0.16	-0.27
EXTR	ERA5 h	-0.45	-0.86	0.02	-0.17	-0.16
	ERA5 d	-0.44	-0.97	-0.17	-0.08	-0.14
	RaKliDa	-0.33	-0.8	-0.26	-0.02	-0.23
	Station	-0.35	-0.66	-0.3	-0.02	-0.18
BR90	ERA5 h	-0.84	-1.98	0.47	-0.29	-0.27
	ERA5 d	-0.82	-1.8	0.48	-0.16	-0.23
	RaKliDa	-0.63	-1.2	0.4	-0.3	-0.15
	Station	-0.68	-0.95	0.22	-0.09	-0.23
CBR90	ERA5 h	0.42	-0.01	0.58	0.27	-0.05
	ERA5 d	0.38	-0.04	0.49	0.28	-0.07
	RaKliDa	0.44	-0.07	0.47	0	0.05
	Station	0.47	-0.02	0.29	0.42	-0.08
Correlation						
GBR90	ERA5 h	0.54	0.2	0.33	0.05	0
	ERA5 d	0.56	0.23	0.37	0.1	-0.01
	RaKliDa	0.51	0.15	0.31	-0.01	0.11
	Station	0.55	0.21	0.11	0.21	0
EXTR	ERA5 h	0.27	0.39	0.3	0.16	0.07
	ERA5 d	0.06	0.29	0.29	0.22	0.06
	RaKliDa	0.16	0.23	0.2	0.33	-0.01
	Station	0.29	0.29	0.17	0.35	0.03
BR90	ERA5 h	0.21	0.06	0.47	0.07	0.01
	ERA5 d	0.17	0.03	0.5	0.13	-0.01
	RaKliDa	0.15	-0.11	0.42	-0.01	0.12
	Station	0.25	0.01	0.25	0.24	-0.01
CBR90	ERA5 h	0.52	0.32	0.6	0.35	0.07
	ERA5 d	0.52	0.36	0.55	0.37	0.07
	RaKliDa	0.55	0.29	0.53	0.24	0.21
	Station	0.56	0.33	0.39	0.46	0.09
BIAS						
GBR90	ERA5 h	0.85	1.15	1.01	3.45	3.93

Отформатировано: английский (Соединенное Королевство)

Отформатировано: английский (Соединенное Королевство)

Отформатировано: английский (Соединенное Королевство)

Отформатировано: английский (Соединенное Королевство)

Отформатировано: английский (Соединенное Королевство)

Отформатировано: английский (Соединенное Королевство)

Отформатировано: английский (Соединенное Королевство)

Отформатировано: английский (Соединенное Королевство)

Отформатировано: английский (Соединенное Королевство)

Отформатировано: английский (Соединенное Королевство)

Отформатировано: английский (Соединенное Королевство)

Отформатировано: английский (Соединенное Королевство)

Отформатировано: английский (Соединенное Королевство)

Отформатировано: английский (Соединенное Королевство)

Отформатировано: английский (Соединенное Королевство)

	ERA5 d	0.9	1.23	0.92	3.16	3.69
	RaKliDa	0.94	1.29	0.88	3.14	3.97
	Station	0.83	1.3	0.9	3.46	3.59
EXTR	ERA5 h	0.76	0.85	0.63	2.91	2.97
	ERA5 d	0.71	0.83	0.54	2.72	2.83
	RaKliDa	0.74	0.95	0.53	2.79	3.11
	Station	0.65	0.98	0.51	3.1	2.91
BR90	ERA5 h	0.57	0.55	0.97	3.15	3.49
	ERA5 d	0.59	0.57	0.9	2.76	3.16
	RaKliDa	0.63	0.64	0.88	2.76	3.47
	Station	0.55	0.69	0.9	3.01	3.11
CBR90	ERA5 h	1.05	1.12	0.96	1.01	2
	ERA5 d	1	1.11	0.81	0.98	1.78
	RaKliDa	1.1	1.2	0.8	0.82	2.01
	Station	0.96	1.24	0.75	1.21	1.62
Variance ratio						
GBR90	ERA5 h	0.42	0.24	1.27	5.85	3.09
	ERA5 d	0.45	0.28	0.73	3.64	1.88
	RaKliDa	0.54	0.33	0.68	5.09	2.07
	Station	0.56	0.33	0.74	3.39	2
EXTR	ERA5 h	0.2	0.13	0.55	3.71	1.55
	ERA5 d	0.24	0.13	0.5	2.83	1.12
	RaKliDa	0.26	0.15	0.51	2.99	1.63
BR90	Station	0.25	0.16	0.58	2.92	1.25
	ERA5 h	0.16	0.07	1.08	5.28	2.5
	ERA5 d	0.17	0.08	0.84	3.05	1.42
	RaKliDa	0.2	0.13	0.8	4.22	1.66
CBR90	Station	0.19	0.15	0.72	2.91	1.53
	ERA5 h	0.57	0.33	1.3	0.56	0.97
	ERA5 d	0.52	0.3	0.96	0.55	0.59
	RaKliDa	0.57	0.32	1.01	0.38	0.73
Station	0.61	0.33	0.83	0.76	0.48	
MAE						
GBR90	ERA5 h	3.08	4.51	4.6	20.09	19.24
	ERA5 d	2.95	4.69	4.17	17.68	17.65
	RaKliDa	3.04	4.97	4.34	17.78	19.04
	Station	3.13	4.83	4.92	20.19	17.09
EXTR	ERA5 h	3.77	3.54	5.67	15.67	13.5
	ERA5 d	4.23	3.86	6.42	14.12	12.6
	RaKliDa	4.03	3.92	6.77	14.66	14.33
	Station	3.96	3.82	7.07	17.21	13.04
BR90	ERA5 h	4.36	4.36	3.96	17.76	16.74
	ERA5 d	4.39	4.48	3.76	14.49	14.61
	RaKliDa	4.33	4.55	4.11	14.92	16.07
	Station	4.42	4.27	4.49	16.53	14.22
CBR90	ERA5 h	3.1	4.21	3.72	3.46	8.4
	ERA5 d	3.14	4.05	4.07	3.38	7.31
	RaKliDa	3.13	4.28	4.23	3.71	8
	Station	2.99	4.27	4.54	3.53	6.18

Отформатировано: английский (Соединенное Королевство)

Отформатировано: английский (Соединенное Королевство)

Отформатировано: английский (Соединенное Королевство)

Отформатировано: английский (Соединенное Королевство)

Отформатировано: английский (Соединенное Королевство)

Отформатировано: английский (Соединенное Королевство)

Отформатировано: английский (Соединенное Королевство)

Отформатировано: английский (Соединенное Королевство)

Отформатировано: английский (Соединенное Королевство)

Отформатировано: английский (Соединенное Королевство)

Отформатировано: английский (Соединенное Королевство)

Отформатировано: английский (Соединенное Королевство)

Отформатировано: английский (Соединенное Королевство)

708 **Data and Code availability**

709 Authors fully support open-source and reproducible research. Therefore, all the data and codes are available as Supplementary  
710 material under the following HydroShare composite resource  
711 <https://doi.org/10.4211/hs.567d7bdc7b84465ca333b6e0c011853a> , which include:

- 712 - Raw eddy-covariance and meteorological measurement daily data with location files
- 713 - Raw results of model runs for each framework, including model calibration and FAO simulations
- 714 - R-scripts to reproduce figures and tables for the manuscript

715 In addition, Global BROOK90 framework is available under [https://github.com/hydrovorobey/Global\\_BROOK90](https://github.com/hydrovorobey/Global_BROOK90),  
716 EXTRUSO framework is available under [https://github.com/GeoinformationSystems/xtruso\\_R](https://github.com/GeoinformationSystems/xtruso_R), and BROOK90 R-version is  
717 available under [https://github.com/rkronen/Brook90\\_R](https://github.com/rkronen/Brook90_R).

718 **Author contribution**

719 Conceptualization VI, LTT and KR; data curation GT, LTT and VI, formal analysis VI, funding acquisition BC, methodology  
720 VI, LTT and KR; supervision KR; visualization VI; writing: original draft preparation VI and LTT, writing: review KR, GT,  
721 BC.

722 **Competing interests**

723 The authors declare that they have no conflict of interest.

724 **Acknowledgements**

725 Authors would like to express great thanks to Uwe Spank for his valuable advises and comments to the paper draft.  
726 Additionally, authors thank BMBF for providing the funding opportunities for the study under the scope of the  
727 ‘KlimaKonform’ project.

728 **References**

729 Ad-hoc-AG Boden: Bodenkundliche Kartieranleitung, Bundesanstalt für Geowissenschaften und Rohstoffe in  
730 Zusammenarbeit mit den Staatlichen Geologischen Dienstender Bundesrepublik Deutschland, Hannover, 2005.  
731 Alessandri, A., Catalano, F., De Felice, M., van den Hurk, B., and Balsamo, G.: Varying snow and vegetation signatures of  
732 surface albedo feedback on the Northern Hemisphere land warming, <https://doi.org/10.1088/1748-9326/abd65f>, 2020.

733 Allen, R., Pereira, L., Raes, D., and Smith, M.: Crop evapotranspiration - Guidelines for computing crop water requirements -  
734 FAO Irrigation and drainage paper 56, FAO - Food and Agriculture Organization of the United Nations, Rome, 1998.

735 Anderson, M. C., Norman, J. M., Mecikalski, J. R., Otkin, J. A., and Kustas, W. P.: A climatological study of  
736 evapotranspiration and moisture stress across the continental United States based on thermal remote sensing: 1. Model  
737 formulation, 112, <https://doi.org/10.1029/2006JD007506>, 2007.

738 Anderson, M. C., Norman, J. M., Kustas, W. P., Houborg, R., Starks, P. J., and Agam, N.: A thermal-based remote sensing  
739 technique for routine mapping of land-surface carbon, water and energy fluxes from field to regional scales, 112, 4227–4241,  
740 <https://doi.org/10.1016/j.rse.2008.07.009>, 2008.

741 Baldocchi, D.: Flux Footprints Within and Over Forest Canopies, *Boundary-Layer Meteorology*, 85, 273–292,  
742 <https://doi.org/10.1023/A:1000472717236>, 1997.

743 Baldocchi, D., Falge, E., Gu, L., Olson, R., Hollinger, D., Running, S., Anthoni, P., Bernhofer, C., Davis, K., Evans, R.,  
744 Fuentes, J., Goldstein, A., Katul, G., Law, B., Lee, X., Malhi, Y., Meyers, T., Munger, W., Oechel, W., U, K. T. P., Pilegaard,  
745 K., Schmid, H. P., Valentini, R., Verma, S., Vesala, T., Wilson, K., and Wofsy, S.: FLUXNET: A New Tool to Study the  
746 Temporal and Spatial Variability of Ecosystem-Scale Carbon Dioxide, Water Vapor, and Energy Flux Densities, 82, 2415–  
747 2434, [https://doi.org/10.1175/1520-0477\(2001\)082<2415:FANTTS>2.3.CO;2](https://doi.org/10.1175/1520-0477(2001)082<2415:FANTTS>2.3.CO;2), 2001.

748 Beven, K. J., Kirkby, M. J., Freer, J. E., and Lamb, R.: A history of TOPMODEL, *Hydrol. Earth Syst. Sci.*, 25, 527–549,  
749 <https://doi.org/10.5194/hess-25-527-2021>, 2021.

750 Bonan, G. B., Patton, E. G., Finnigan, J. J., Baldocchi, D. D., and Harman, I. N.: Moving beyond the incorrect but useful  
751 paradigm: reevaluating big-leaf and multilayer plant canopies to model biosphere-atmosphere fluxes – a review, *Agricultural  
752 and Forest Meteorology*, 306, 108435, <https://doi.org/10.1016/j.agrformet.2021.108435>, 2021.

753 Boulet, G., Mougnot, B., Lhomme, J.-P., Fanise, P., Lili-Chabaane, Z., Oliosio, A., Bahir, M., Rivalland, V., Jarlan, L., Merlin,  
754 O., Coudert, B., Er-Raki, S., and Lagouarde, J.-P.: The SPARSE model for the prediction of water stress and evapotranspiration  
755 components from thermal infra-red data and its evaluation over irrigated and rainfed wheat, *Hydrol. Earth Syst. Sci.*, 19, 4653–  
756 4672, <https://doi.org/10.5194/hess-19-4653-2015>, 2015.

757 Buchhorn, M., Smets, B., Bertels, L., Lesiv, M., Tsendbazar, N.-E., Herold, M., and Fritz, S.: Copernicus Global Land Service:  
758 Land Cover 100m: collection 3: epoch 2019: Globe 2020., 2020.

759 Carminati, A. and Javaux, M.: Soil Rather Than Xylem Vulnerability Controls Stomatal Response to Drought, *Trends in Plant  
760 Science*, 25, 868–880, <https://doi.org/10.1016/j.tplants.2020.04.003>, 2020.

761 Cerro, R. T. G. del, Subathra, M. S. P., Kumar, N. M., Verrastro, S., and George, S. T.: Modelling the daily reference  
762 evapotranspiration in semi-arid region of South India: A case study comparing ANFIS and empirical models, 8, 173–184,  
763 <https://doi.org/10.1016/j.inpa.2020.02.003>, 2021.

764 Chang, L.-L., Dwivedi, R., Knowles, J. F., Fang, Y.-H., Niu, G.-Y., Pelletier, J. D., Rasmussen, C., Durcik, M., Barron-  
765 Gafford, G. A., and Meixner, T.: Why Do Large-Scale Land Surface Models Produce a Low Ratio of Transpiration to  
766 Evapotranspiration?, 123, 9109–9130, <https://doi.org/10.1029/2018JD029159>, 2018.

767 Copernicus Climate Change Service (C3S): ERA5: Fifth generation of ECMWF atmospheric reanalyses of the global climate.  
768 ERA5 hourly data on single levels from 1979 to present.: 10.24381/cds.adbb2d47, last access: 14 February 2022.

769 Dijk, A. I. J. M. van, Gash, J. H., Gorsel, E. van, Blanken, P. D., Cescatti, A., Emmel, C., Gielen, B., Harman, I. N., Kiely, G.,  
770 Merbold, L., Montagnani, L., Moors, E., Sottocornola, M., Varlagin, A., Williams, C. A., and Wohlfahrt, G.: Rainfall  
771 interception and the coupled surface water and energy balance, 214–215, 402–415,  
772 <https://doi.org/10.1016/j.agrformet.2015.09.006>, 2015.

773 Drought 2018 Team and COS Ecosystem Thematic Centre: Drought-2018 ecosystem eddy covariance flux product for 52  
774 stations in FLUXNET-Archive format, 2020.

775 Efstratiadis, A. and Koutsoyiannis, D.: The multiobjective evolutionary annealing-simplex method and its application in  
776 calibrating hydrological models, in: Geophysical Research Abstracts, Conference: European Geosciences Union General  
777 Assembly, Vienna, Austria, <http://dx.doi.org/10.13140/RG.2.2.32963.81446>, 2005.

778 European Environment Agency: Corine Land Cover (CLC) 2012, Version 2020\_20u1, 2020.

779 Federer, A. and Douglas, L.: Brook: A Hydrologic Simulation Model for Eastern Forests, 2nd ed., Water Resource Research  
780 Center University of New Hampshire, Durham, New Hampshire, 1983.

781 Federer, C. A.: BROOK 90: A simulation model for evaporation, soil water, and streamflow., 2002.

782 Federer, C. A., Vörösmarty, C., and Fekete, B.: Sensitivity of Annual Evaporation to Soil and Root Properties in Two Models  
783 of Contrasting Complexity, 4, 1276–1290, [https://doi.org/10.1175/1525-7541\(2003\)004<1276:SOAETS>2.0.CO;2](https://doi.org/10.1175/1525-7541(2003)004<1276:SOAETS>2.0.CO;2), 2003.

784 Feng, Y., Cui, N., Zhao, L., Hu, X., and Gong, D.: Comparison of ELM, GANN, WNN and empirical models for estimating  
785 reference evapotranspiration in humid region of Southwest China, 536, 376–383,  
786 <https://doi.org/10.1016/j.jhydrol.2016.02.053>, 2016.

787 Fisher, J. B., Melton, F., Middleton, E., Hain, C., Anderson, M., Allen, R., McCabe, M. F., Hook, S., Baldocchi, D., Townsend,  
788 P. A., Kilic, A., Tu, K., Miralles, D. D., Perret, J., Lagouarde, J.-P., Waliser, D., Purdy, A. J., French, A., Schimel, D.,  
789 Famiglietti, J. S., Stephens, G., and Wood, E. F.: The future of evapotranspiration: Global requirements for ecosystem  
790 functioning, carbon and climate feedbacks, agricultural management, and water resources, 53, 2618–2626,  
791 <https://doi.org/10.1002/2016WR020175>, 2017.

792 Foken, T.: The Energy Balance Closure Problem: An Overview, 18, 1351–1367, 2008.

793 Groh, J., Puhlmann, H., and Wilpert, K.: Calibration of a soil-water balance model with a combined objective function for the  
794 optimization of the water retention curve, Hydrologie und Wasserbewirtschaftung, 57, 152–162,  
795 <https://doi.org/10.5675/HyWa-2013,4-1>, 2013.

796 Gupta, H. V., Kling, H., Yilmaz, K. K., and Martinez, G. F.: Decomposition of the mean squared error and NSE performance  
797 criteria: Implications for improving hydrological modelling, 377, 80–91, <https://doi.org/10.1016/j.jhydrol.2009.08.003>, 2009.

798 Habel, R., Puhlmann, H., and Müller, A.-C.: The water budget of forests the big unknown outside of our intensive monitoring  
799 plots?, FORECOMON 2021, Birmensdorf, Switzerland, 2021.



800 Haddeland, I., Clark, D. B., Franssen, W., Ludwig, F., Voß, F., Arnell, N. W., Bertrand, N., Best, M., Folwell, S., Gerten, D.,  
801 Gomes, S., Gosling, S. N., Hagemann, S., Hanasaki, N., Harding, R., Heinke, J., Kabat, P., Koirala, S., Oki, T., Polcher, J.,  
802 Stacke, T., Viterbo, P., Weedon, G. P., and Yeh, P.: Multimodel Estimate of the Global Terrestrial Water Balance: Setup and  
803 First Results, *Journal of Hydrometeorology*, 12, 869–884, <https://doi.org/10.1175/2011JHM1324.1>, 2011.

804 Harding, R., Best, M., Blyth, E., Hagemann, S., Kabat, P., Tallaksen, L. M., Warnaars, T., Wiberg, D., Weedon, G. P., van  
805 Lanen, H., Ludwig, F., and Haddeland, I.: WATCH: Current Knowledge of the Terrestrial Global Water Cycle, 12, 1149–  
806 1156, 2011.

807 Hengl, T., Mendes de Jesus, J., Heuvelink, G. B. M., Ruiperez Gonzalez, M., Kilibarda, M., Blagotić, A., Shangguan, W.,  
808 Wright, M. N., Geng, X., Bauer-Marschallinger, B., Guevara, M. A., Vargas, R., MacMillan, R. A., Batjes, N. H., Leenaars,  
809 J. G. B., Ribeiro, E., Wheeler, I., Mantel, S., and Kempen, B.: SoilGrids250m: Global gridded soil information based on  
810 machine learning, 12, 1–40, <https://doi.org/10.1371/journal.pone.0169748>, 2017.

811 Hoek van Dijke, A. J., Mallick, K., Schlerf, M., Machwitz, M., Herold, M., and Teuling, A. J.: Examining the link between  
812 vegetation leaf area and land–atmosphere exchange of water, energy, and carbon fluxes using FLUXNET data, 17, 4443–4457,  
813 <https://doi.org/10.5194/bg-17-4443-2020>, 2020.

814 Hollinger, D. Y. and Richardson, A. D.: Uncertainty in eddy covariance measurements and its application to physiological  
815 models, *Tree Physiology*, 25, 873–885, <https://doi.org/10.1093/treephys/25.7.873>, 2005.

816 Imukova, K., Ingwersen, J., Hevart, M., and Streck, T.: Energy balance closure on a winter wheat stand: comparing the eddy  
817 covariance technique with the soil water balance method, 13, 63–75, <https://doi.org/10.5194/bg-13-63-2016>, 2016.

818 Jung, M., Reichstein, M., Margolis, H. A., Cescatti, A., Richardson, A. D., Arain, M. A., Arneth, A., Bernhofer, C., Bonal, D.,  
819 Chen, J., Gianelle, D., Gobron, N., Kiely, G., Kutsch, W., Lasslop, G., Law, B. E., Lindroth, A., Merbold, L., Montagnani, L.,  
820 Moors, E. J., Papale, D., Sottocornola, M., Vaccari, F., and Williams, C.: Global patterns of land-atmosphere fluxes of carbon  
821 dioxide, latent heat, and sensible heat derived from eddy covariance, satellite, and meteorological observations, 116,  
822 <https://doi.org/10.1029/2010JG001566>, 2011.

823 Kottek, M., Grieser, J., Beck, C., Rudolf, B., and Rubel, F.: World Map of the Köppen-Geiger climate classification updated,  
824 15, 259–263, <https://doi.org/10.1127/0941-2948/2006/0130>, 2006.

825 Kronenberg, R. and Bernhofer, C.: A method to adapt radar-derived precipitation fields for climatological applications, 22,  
826 636–649, <https://doi.org/10.1002/met.1498>, 2015.

827 Kronenberg, R. and Oehlschlägel, L. M.: BROOK90 in R, 2019.

828 Lawrence, D. M., Thornton, P. E., Oleson, K. W., and Bonan, G. B.: The Partitioning of Evapotranspiration into Transpiration,  
829 Soil Evaporation, and Canopy Evaporation in a GCM: Impacts on Land–Atmosphere Interaction, 8, 862–880,  
830 <https://doi.org/10.1175/JHM596.1>, 2007.

831 Leaf, C. and Brink, G.: Hydrologic simulation model of Colorado subalpine forest, Forest Service, U.S. Dept. of Agriculture,  
832 1973.

833 Lehmann, P., Merlin, O., Gentine, P., and Or, D.: Soil Texture Effects on Surface Resistance to Bare-Soil Evaporation,  
834 Geophysical Research Letters, 45, 10,398-10,405, <https://doi.org/10.1029/2018GL078803>, 2018.

835 Leuning, R., Zhang, Y. Q., Rajaud, A., Cleugh, H., and Tu, K.: A simple surface conductance model to estimate regional  
836 evaporation using MODIS leaf area index and the Penman-Monteith equation, 44, <https://doi.org/10.1029/2007WR006562>,  
837 2008.

838 Lide, D.: CRC Handbook of Chemistry and Physics, 85th ed., CRC Press, 2005.

839 Liu, M., Bárdossy, A., Li, J., and Jiang, Y.: Physically-based modeling of topographic effects on spatial evapotranspiration  
840 and soil moisture patterns through radiation and wind, Hydrol. Earth Syst. Sci., 16, 357–373, <https://doi.org/10.5194/hess-16->  
841 357-2012, 2012.

842 Luo, X., Chen, J. M., Liu, J., Black, T. A., Croft, H., Staebler, R., He, L., Arain, M. A., Chen, B., Mo, G., Gonsamo, A., and  
843 McCaughey, H.: Comparison of Big-Leaf, Two-Big-Leaf, and Two-Leaf Upscaling Schemes for Evapotranspiration  
844 Estimation Using Coupled Carbon-Water Modeling, Journal of Geophysical Research: Biogeosciences, 123, 207–225,  
845 <https://doi.org/10.1002/2017JG003978>, 2018.

846 Luong, T. T., Pöschmann, J., Vorobevskii, I., Wiemann, S., Kronenberg, R., and Bernhofer, C.: Pseudo-Spatially-Distributed  
847 Modeling of Water Balance Components in the Free State of Saxony, 7, <https://doi.org/10.3390/hydrology7040084>, 2020.

848 Mallick, K., Toivonen, E., Trebs, I., Boegh, E., Cleverly, J., Eamus, D., Koivusalo, H., Drewry, D., Arndt, S. K., Griebel, A.,  
849 Beringer, J., and Garcia, M.: Bridging Thermal Infrared Sensing and Physically-Based Evapotranspiration Modeling: From  
850 Theoretical Implementation to Validation Across an Aridity Gradient in Australian Ecosystems, 54, 3409–3435,  
851 <https://doi.org/10.1029/2017WR021357>, 2018.

852 Mapzen Data Products: Amazon Web Service Terrain Tiles, 2020.

853 Martens, B., De Jeu, R. A. M., Verhoest, N. E. C., Schuurmans, H., Kleijer, J., and Miralles, D. G.: Towards Estimating Land  
854 Evaporation at Field Scales Using GLEAM, 10, <https://doi.org/10.3390/rs10111720>, 2018.

855 Mauder, M., Genzel, S., Fu, J., Kiese, R., Soltani, M., Steinbrecher, R., Zeeman, M., Banerjee, T., De Roo, F., and Kunstmann,  
856 H.: Evaluation of energy balance closure adjustment methods by independent evapotranspiration estimates from lysimeters  
857 and hydrological simulations, 32, 39–50, <https://doi.org/10.1002/hyp.11397>, 2018.

858 McDonald, J. E.: On the Ratio of Evaporation to Precipitation, 42, 185–189, 1961.

859 McNally, A., McCartney, S., Ruane, A. C., Mladenova, I. E., Whitcraft, A. K., Becker-Reshef, I., Bolten, J. D., Peters-Lidard,  
860 C. D., Rosenzweig, C., and Uz, S. S.: Hydrologic and Agricultural Earth Observations and Modeling for the Water-Food  
861 Nexus, 7, 23, <https://doi.org/10.3389/fenvs.2019.00023>, 2019.

862 BingTM Maps tiles: <http://ecn.t3.tiles.virtualearth.net/tiles/a{q}.jpeg?g=1>, last access: 15 February 2020.

863 Miralles, D. G., Holmes, T. R. H., De Jeu, R. A. M., Gash, J. H., Meesters, A. G. C. A., and Dolman, A. J.: Global land-surface  
864 evaporation estimated from satellite-based observations, 15, 453–469, <https://doi.org/10.5194/hess-15-453-2011>, 2011.

865 Miralles, D. G., Jiménez, C., Jung, M., Michel, D., Ershadi, A., McCabe, M. F., Hirschi, M., Martens, B., Dolman, A. J.,  
866 Fisher, J. B., Mu, Q., Seneviratne, S. I., Wood, E. F., and Fernández-Prieto, D.: The WACMOS-ET project – Part 2: Evaluation

867 of global terrestrial evaporation data sets, *Hydrol. Earth Syst. Sci.*, 20, 823–842, <https://doi.org/10.5194/hess-20-823-2016>,  
868 2016.

869 Moorhead, J. E., Marek, G. W., Gowda, P. H., Lin, X., Colaizzi, P. D., Evett, S. R., and Kutikoff, S.: Evaluation of  
870 Evapotranspiration from Eddy Covariance Using Large Weighing Lysimeters, 9, <https://doi.org/10.3390/agronomy9020099>,  
871 2019.

872 Mueller, B., Seneviratne, S. I., Jimenez, C., Corti, T., Hirschi, M., Balsamo, G., Ciais, P., Dirmeyer, P., Fisher, J. B., Guo, Z.,  
873 Jung, M., Maignan, F., McCabe, M. F., Reichle, R., Reichstein, M., Rodell, M., Sheffield, J., Teuling, A. J., Wang, K., Wood,  
874 E. F., and Zhang, Y.: Evaluation of global observations-based evapotranspiration datasets and IPCC AR4 simulations, 38,  
875 <https://doi.org/10.1029/2010GL046230>, 2011.

876 Müller Schmied, H., Adam, L., Eisner, S., Fink, G., Flörke, M., Kim, H., Oki, T., Portmann, F. T., Reinecke, R., Riedel, C.,  
877 Song, Q., Zhang, J., and Döll, P.: Variations of global and continental water balance components as impacted by climate  
878 forcing uncertainty and human water use, *Hydrol. Earth Syst. Sci.*, 20, 2877–2898, <https://doi.org/10.5194/hess-20-2877-2016>,  
879 2016.

880 Murray, F. W.: On the Computation of Saturation Vapor Pressure, 6, 203–204, [https://doi.org/10.1175/1520-0450\(1967\)006<0203:OTCOSV>2.0.CO;2](https://doi.org/10.1175/1520-0450(1967)006<0203:OTCOSV>2.0.CO;2), 1967.

882 Myhre, G. and Myhre, A.: Uncertainties in Radiative Forcing due to Surface Albedo Changes Caused by Land-Use Changes,  
883 *Journal of Climate*, 16, 1511–1524, [https://doi.org/10.1175/1520-0442\(2003\)016<1511:UIRFDT>2.0.CO;2](https://doi.org/10.1175/1520-0442(2003)016<1511:UIRFDT>2.0.CO;2), 2003.

884 Myneni, R., Knyazikhin, Y., and Park, T.: MCD15A2H MODIS/Terra+Aqua Leaf Area Index/FPAR 8-day L4 Global 500m  
885 SIN Grid V006, 2015.

886 Nash, J. E. and Sutcliffe, J. V.: River flow forecasting through conceptual models part I — A discussion of principles, 10,  
887 282–290, [https://doi.org/10.1016/0022-1694\(70\)90255-6](https://doi.org/10.1016/0022-1694(70)90255-6), 1970.

888 Planet dump retrieved from <https://planet.osm.org>: <https://www.openstreetmap.org>.

889 Page, J.: 1 - The Role of Solar Radiation Climatology in the Design of Photovoltaic Systems, in: *Practical Handbook of*  
890 *Photovoltaics*, edited by: Markvart, T. and Castañer, L., Elsevier Science, Amsterdam, 5–66, <https://doi.org/10.1016/B978-185617390-2/50004-0>, 2003.

892 Pan, S., Pan, N., Tian, H., Friedlingstein, P., Sitch, S., Shi, H., Arora, V. K., Haverd, V., Jain, A. K., Kato, E., Lienert, S.,  
893 Lombardozi, D., Nabel, J. E. M. S., Otlé, C., Poulter, B., Zaehle, S., and Running, S. W.: Evaluation of global terrestrial  
894 evapotranspiration using state-of-the-art approaches in remote sensing, machine learning and land surface modeling, *Hydrol.*  
895 *Earth Syst. Sci.*, 24, 1485–1509, <https://doi.org/10.5194/hess-24-1485-2020>, 2020.

896 Paredes, P., Pereira, L. S., Almorox, J., and Darouich, H.: Reference grass evapotranspiration with reduced data sets:  
897 Parameterization of the FAO Penman-Monteith temperature approach and the Hargeaves-Samani equation using local climatic  
898 variables, *Agricultural Water Management*, 240, 106210, <https://doi.org/10.1016/j.agwat.2020.106210>, 2020.

899 Park, S. and Park, S. K.: Parameterization of the snow-covered surface albedo in the Noah-MP Version 1.0 by implementing  
900 vegetation effects, 9, 1073–1085, <https://doi.org/10.5194/gmd-9-1073-2016>, 2016.

901 Pastorello, G., Trotta, C., Canfora, E., Chu, H., Christianson, D., Cheah, Y.-W., Poindexter, C., Chen, J., Elbashandy, A.,  
902 Humphrey, M., Isaac, P., Polidori, D., Reichstein, M., Ribeca, A., van Ingen, C., Vuichard, N., Zhang, L., Amiro, B., Ammann,  
903 C., Arain, M. A., Ardö, J., Arkebauer, T., Arndt, S. K., Arriga, N., Aubinet, M., Aurela, M., Baldocchi, D., Barr, A.,  
904 Beamesderfer, E., Marchesini, L. B., Bergeron, O., Beringer, J., Bernhofer, C., Berveiller, D., Billesbach, D., Black, T. A.,  
905 Blanken, P. D., Bohrer, G., Boike, J., Bolstad, P. V., Bonal, D., Bonnefond, J.-M., Bowling, D. R., Bracho, R., Brodeur, J.,  
906 Brümmer, C., Buchmann, N., Burban, B., Burns, S. P., Buysse, P., Cale, P., Cavagna, M., Cellier, P., Chen, S., Chini, I.,  
907 Christensen, T. R., Cleverly, J., Collalti, A., Consalvo, C., Cook, B. D., Cook, D., Coursolle, C., Cremonese, E., Curtis, P. S.,  
908 D'Andrea, E., da Rocha, H., Dai, X., Davis, K. J., Cinti, B. D., Grandcourt, A. de Ligne, A. D., De Oliveira, R. C., Delpierre,  
909 N., Desai, A. R., Di Bella, C. M., Tommasi, P. di, Dolman, H., Domingo, F., Dong, G., Dore, S., Duce, P., Dufrêne, E., Dunn,  
910 A., Dušek, J., Eamus, D., Eichelmann, U., ElKhidir, H. A. M., Eugster, W., Ewenz, C. M., Ewers, B., Famulari, D., Fares, S.,  
911 Feigenwinter, I., Feitz, A., Fensholt, R., Filippa, G., Fischer, M., Frank, J., Galvagno, M., et al.: The FLUXNET2015 dataset  
912 and the ONEFlux processing pipeline for eddy covariance data, *Scientific Data*, 7, 225. [https://doi.org/10.1038/s41597-020-](https://doi.org/10.1038/s41597-020-0534-3)  
913 [0534-3](https://doi.org/10.1038/s41597-020-0534-3), 2020.

914 Perez-Priego, O., El-Madany, T. S., Migliavacca, M., Kowalski, A. S., Jung, M., Carrara, A., Kolle, O., Martín, M. P., Pacheco-  
915 Labrador, J., Moreno, G., and Reichstein, M.: Evaluation of eddy covariance latent heat fluxes with independent lysimeter and  
916 sapflow estimates in a Mediterranean savannah ecosystem, *Agricultural and Forest Meteorology*, 236, 87–99,  
917 <https://doi.org/10.1016/j.agrformet.2017.01.009>, 2017.

918 Potapov, P., Li, X., Hernandez-Serna, A., Tyukavina, A., Hansen, M. C., Kommareddy, A., Pickens, A., Turubanova, S., Tang,  
919 H., Silva, C. E., Armston, J., Dubayah, R., Blair, J. B., and Hofton, M.: Mapping global forest canopy height through  
920 integration of GEDI and Landsat data, *Remote Sensing of Environment*, 253, 112165,  
921 <https://doi.org/10.1016/j.rse.2020.112165>, 2021.

922 Pypker, T. G., Bond, B. J., Link, T. E., Marks, D., and Unsworth, M. H.: The importance of canopy structure in controlling  
923 the interception loss of rainfall: Examples from a young and an old-growth Douglas-fir forest, *Agricultural and Forest*  
924 *Meteorology*, 130, 113–129, <https://doi.org/10.1016/j.agrformet.2005.03.003>, 2005.

925 Raupach, M. and Finnigan, J.: “Single-Layer Models of Evaporation From Plant Canopies Are Incorrect but Useful, Whereas  
926 Multilayer Models Are Correct but Useless”: Discuss, *Functional Plant Biol.*, 15, 705–716, 1988.

927 Reed, P. and Devireddy, V.: Groundwater monitoring design: a case study combining epsilon dominance archiving and  
928 automatic parameterization for the NSGA-II, in: *Applications of Multi-Objective Evolutionary Algorithms*, 79–100,  
929 [https://doi.org/10.1142/9789812567796\\_0004](https://doi.org/10.1142/9789812567796_0004), 2004.

930 Richardson, A. D., Aubinet, M., Barr, A. G., Hollinger, D. Y., Ibrom, A., Lasslop, G., and Reichstein, M.: Uncertainty  
931 Quantification, in: *Eddy Covariance: A Practical Guide to Measurement and Data Analysis*, edited by: Aubinet, M., Vesala,  
932 T., and Papale, D., Springer Netherlands, Dordrecht, 173–209, [https://doi.org/10.1007/978-94-007-2351-1\\_7](https://doi.org/10.1007/978-94-007-2351-1_7), 2012.

933 Richter, D.: Ergebnisse methodischer Untersuchungen zur Korrektur des systematischen Meßfehlers des Hellmann-  
934 Niederschlagsmessers von Dieter Richter, *Deutscher Wetterdienst*, Offenbach am Main, 1995.

935 Rudd, A. C. and Kay, A. L.: Use of very high resolution climate model data for hydrological modelling: estimation of potential  
936 evaporation, *Hydrology Research*, 47, 660–670, <https://doi.org/10.2166/nh.2015.028>, 2015.

937 Sächsisches Landesamt für Umwelt, Landwirtschaft und Geologie: Bodenkarte 1 : 50.000, 2020.

938 Schulz, S., Becker, R., Richard-Cerda, J. C., Usman, M., aus der Beek, T., Merz, R., and Schüth, C.: Estimating water balance  
939 components in irrigated agriculture using a combined approach of soil moisture and energy balance monitoring, and numerical  
940 modelling, 35, e14077, <https://doi.org/10.1002/hyp.14077>, 2021.

941 Schwärzel, K., Feger, K.-H., Häntzschel, J., Menzer, A., Spank, U., Clausnitzer, F., Köstner, B., and Bernhofer, C.: A novel  
942 approach in model-based mapping of soil water conditions at forest sites, 258, 2163–2174,  
943 <https://doi.org/10.1016/j.foreco.2009.03.033>, 2009.

944 Sentelhas, P. C., Gillespie, T. J., and Santos, E. A.: Evaluation of FAO Penman–Monteith and alternative methods for  
945 estimating reference evapotranspiration with missing data in Southern Ontario, Canada, *Agricultural Water Management*, 97,  
946 635–644, <https://doi.org/10.1016/j.agwat.2009.12.001>, 2010.

947 Shuttleworth, W. J. and Wallace, J. S.: Evaporation from sparse crops—an energy combination theory, 111, 839–855,  
948 <https://doi.org/10.1002/qj.49711146910>, 1985.

949 Spank, U., Schwärzel, K., Renner, M., Moderow, U., and Bernhofer, C.: Effects of measurement uncertainties of  
950 meteorological data on estimates of site water balance components, 492, 176–189,  
951 <https://doi.org/10.1016/j.jhydrol.2013.03.047>, 2013.

952 Staatsbetrieb Geobasisinformation und Vermessung Sachsen: Digitales Geländemodell Sachsen 10 m, 2020.

953 Su, H., McCabe, M. F., Wood, E. F., Su, Z., and Prueger, J. H.: Modeling Evapotranspiration during SMACEX: Comparing  
954 Two Approaches for Local- and Regional-Scale Prediction, 6, 910–922, <https://doi.org/10.1175/JHM466.1>, 2005.

955 Twine, T. E., Kustas, W. P., Norman, J. M., Cook, D. R., Houser, P. R., Meyers, T. P., Prueger, J. H., Starks, P. J., and Wesely,  
956 M. L.: Correcting eddy-covariance flux underestimates over a grassland, *Agricultural and Forest Meteorology*, 103, 279–300,  
957 [https://doi.org/10.1016/S0168-1923\(00\)00123-4](https://doi.org/10.1016/S0168-1923(00)00123-4), 2000.

958 Verhoef, A. and Egea, G.: Modeling plant transpiration under limited soil water: Comparison of different plant and soil  
959 hydraulic parameterizations and preliminary implications for their use in land surface models, *Agricultural and Forest  
960 Meteorology*, 191, 22–32, <https://doi.org/10.1016/j.agrformet.2014.02.009>, 2014.

961 Vilhar, U.: Comparison of drought stress indices in beech forests: a modelling study, 635–642,  
962 <https://doi.org/10.3832/ifor1630-008>, 2016.

963 Vorobevskii, I., Kronenberg, R., and Bernhofer, C.: Global BROOK90 R Package: An Automatic Framework to Simulate the  
964 Water Balance at Any Location, 12, <https://doi.org/10.3390/w12072037>, 2020.

965 Wackernagel, H.: *Multivariate Geostatistics: an Introduction with Applications*, 3rd ed., Springer-Verlag, Berlin Heidelberg,  
966 388 pp., 2003.

967 Wang, S., Pan, M., Mu, Q., Shi, X., Mao, J., Brümmer, C., Jassal, R. S., Krishnan, P., Li, J., and Black, T. A.: Comparing  
968 Evapotranspiration from Eddy Covariance Measurements, Water Budgets, Remote Sensing, and Land Surface Models over  
969 Canada, *Journal of Hydrometeorology*, 16, 1540–1560, <https://doi.org/10.1175/JHM-D-14-0189.1>, 2015.

970 Wang, Z., Schaaf, C. B., Sun, Q., Kim, J., Erb, A. M., Gao, F., Román, M. O., Yang, Y., Petroy, S., Taylor, J. R., Masek, J.  
971 G., Morisette, J. T., Zhang, X., and Papuga, S. A.: Monitoring land surface albedo and vegetation dynamics using high spatial  
972 and temporal resolution synthetic time series from Landsat and the MODIS BRDF/NBAR/albedo product, *International  
973 Journal of Applied Earth Observation and Geoinformation*, 59, 104–117, <https://doi.org/10.1016/j.jag.2017.03.008>, 2017.

974 Warm Winter 2020 Team and COS Ecosystem Thematic Centre: Warm Winter 2020 ecosystem eddy covariance flux product  
975 for 73 stations in FLUXNET-Archive format—release 2022-1 (Version 1.0). ICOS Carbon Portal, 2022.

976 Wegehenkel, M. and Gerke, H. H.: Comparison of real evapotranspiration measured by weighing lysimeters with simulations  
977 based on the Penman formula and a crop growth model, 61, 161–172, <https://doi.org/10.2478/johh-2013-0021>, 2013.

978 Wei, Z., Yoshimura, K., Wang, L., Miralles, D. G., Jasechko, S., and Lee, X.: Revisiting the contribution of transpiration to  
979 global terrestrial evapotranspiration, 44, 2792–2801, <https://doi.org/10.1002/2016GL072235>, 2017.

980 Widmoser, P. and Michel, D.: Partial energy balance closure of eddy covariance evaporation measurements using concurrent  
981 lysimeter observations over grassland, 25, 1151–1163, <https://doi.org/10.5194/hess-25-1151-2021>, 2021.

982 Wilson, K., Goldstein, A., Falge, E., Aubinet, M., Baldocchi, D., Berbigier, P., Bernhofer, C., Ceulemans, R., Dolman, H.,  
983 Field, C., Grelle, A., Ibrom, A., Law, B. E., Kowalski, A., Meyers, T., Moncrieff, J., Monson, R., Oechel, W., Tenhunen, J.,  
984 Valentini, R., and Verma, S.: Energy balance closure at FLUXNET sites, *Agricultural and Forest Meteorology*, 113, 223–243,  
985 [https://doi.org/10.1016/S0168-1923\(02\)00109-0](https://doi.org/10.1016/S0168-1923(02)00109-0), 2002.

986 Wilson, K. B., Hanson, P. J., Mulholland, P. J., Baldocchi, D. D., and Wullschlegel, S. D.: A comparison of methods for  
987 determining forest evapotranspiration and its components: sap-flow, soil water budget, eddy covariance and catchment water  
988 balance, 106, 153–168, [https://doi.org/10.1016/S0168-1923\(00\)00199-4](https://doi.org/10.1016/S0168-1923(00)00199-4), 2001.

989 Winter, J. M. and Eltahir, E. A. B.: The Sensitivity of Latent Heat Flux to Changes in the Radiative Forcing: A Framework for  
990 Comparing Models and Observations, 23, 2345–2356, <https://doi.org/10.1175/2009JCLI3158.1>, 2010.

991 Wu, J., Liu, L., Sun, C., Su, Y., Wang, C., Yang, J., Liao, J., He, X., Li, Q., Zhang, C., and Zhang, H.: Estimating Rainfall  
992 Interception of Vegetation Canopy from MODIS Imageries in Southern China, 11, <https://doi.org/10.3390/rs11212468>, 2019.

993 Yan, H., Wang, S. Q., Billesbach, D., Oechel, W., Zhang, J. H., Meyers, T., Martin, T. A., Matamala, R., Baldocchi, D.,  
994 Bohrer, G., Dragoni, D., and Scott, R.: Global estimation of evapotranspiration using a leaf area index-based surface energy  
995 and water balance model, *Remote Sensing of Environment*, 124, 581–595, <https://doi.org/10.1016/j.rse.2012.06.004>, 2012.

996 Yang, B., Lee, D. K., Heo, H. K., and Biging, G.: The effects of tree characteristics on rainfall interception in urban areas,  
997 *Landscape and Ecological Engineering*, 15, 289–296, <https://doi.org/10.1007/s11355-019-00383-w>, 2019.

998 Zeng, Z., Piao, S., Lin, X., Yin, G., Peng, S., Ciais, P., and Myneni, R. B.: Global evapotranspiration over the past three  
999 decades: estimation based on the water balance equation combined with empirical models, 7, 014026,  
1000 <https://doi.org/10.1088/1748-9326/7/1/014026>, 2012.

1001 Zhang, Y., Leuning, R., Hutley, L. B., Beringer, J., McHugh, I., and Walker, J. P.: Using long-term water balances to  
1002 parameterize surface conductances and calculate evaporation at 0.05° spatial resolution, 46,  
1003 <https://doi.org/10.1029/2009WR008716>, 2010.

1004 Zhang, Y., Chiew, F. H. S., Peña-Arancibia, J., Sun, F., Li, H., and Leuning, R.: Global variation of transpiration and soil  
1005 evaporation and the role of their major climate drivers, *Journal of Geophysical Research: Atmospheres*, 122, 6868–6881,  
1006 <https://doi.org/10.1002/2017JD027025>, 2017.

1007 Zink, M., Kumar, R., Cuntz, M., and Samaniego, L.: A high-resolution dataset of water fluxes and states for Germany  
1008 accounting for parametric uncertainty, *Hydrol. Earth Syst. Sci.*, 21, 1769–1790, <https://doi.org/10.5194/hess-21-1769-2017>,  
1009 2017.

1010